

Accounts

Interfacial Nanochemistry in Liquid–Liquid Extraction Systems

Hitoshi Watarai,* Satoshi Tsukahara, Hirohisa Nagatani,[†] and Akira Ohashi^{††}

Department of Chemistry, Graduate School of Science, Osaka University, Toyonaka, Osaka 560-0043

[†]Department of Natural Science, Hyogo University of Teacher Education, Yashiro, Hyogo 673-1494

^{††}Department of Environmental Sciences, Faculty of Science, Ibaraki University, Mito 310-8512

(Received March 3, 2003)

Recent development of the interfacial nanochemistry in the solvent extraction systems is reviewed, as well as the development of measurement methods for interfacial reactions. The studies on specific reactions at the interface of various metal extraction systems have elucidated essential modes of the interfacial reactions, including the interfacial adsorption, the interfacial complexation, and the interfacial aggregation. The catalytic role of the liquid–liquid interface in the solvent extraction kinetics and the molecular recognition ability of the self-assembled metal complexes at the interface were emphasized. Spectroscopic studies on the rotational and translational dynamics of fluorescent molecules, a single molecule in some cases, at the interface are also discussed. The utility of the molecular dynamics simulations is demonstrated in the discussions of the solvent structure in the interfacial region and of the stability of surface active molecules at the interface.

The liquid–liquid interface is a boundary of two immiscible solvents; it occurs very frequently in oil–water systems. The properties of water and of organic phases are found in the two-dimensional boundary with a thickness of only 1 nm.¹ The liquid–liquid system is utilized for the separation and syntheses in various fields of chemistry and chemical engineering, e.g. solvent extraction of metal ions and protein. Various organic and inorganic compounds have been separated or concentrated by solvent extraction method. Since the 1970's, the role of the interface in the solvent extraction kinetics has been one point of disagreement. However, there was no effective method to measure the interfacial concentration and its change as a function of time.^{2,3} Since the 1980's, several new methods have been invented; these have contributed to a break-through in the study of interfaces in solvent extraction systems.⁴

The solvent extraction process of metal ions depends inherently on the mass transfer across the interface. Therefore, the elucidation of the kinetic role of the interface is very important to understand the extraction mechanism and to control the extraction rates. In the beginning of the 1980's, the high-speed stirring (HSS) method was invented by Watarai and Freiser.^{5,6} Other new methods have been proposed one after another. These included the two-phase stopped flow method,⁷ the capillary plate method,⁸ total internal reflection spectrometry,^{9,10} the centrifugal liquid membrane (CLM) method,¹¹ and the two-phase sheath flow method.¹²

By using the newly developed methods, the specific roles of liquid–liquid interfaces have been discovered. The catalytic

role of the interface in the solvent extraction kinetics was observed in various extraction systems. Interfacial adsorption of the extractant or an intermediate complex at the liquid–liquid interface made the extraction rate much faster. Interfacial accumulation or concentration of adsorbed molecules is another specific role of the interface. Interfacial aggregation of metal complexes, which was observed very frequently in the solvent extraction systems, has been studied in detail by the new methods. Dynamic behavior of adsorbed molecules was examined by means of various experimental approaches including the time-resolved fluorescence method, the second harmonic generation method and the single molecule probing method. The utility of molecular dynamics simulation for depicting molecular motions around the interface is also demonstrated.

Development of Measurement Techniques of Interfacial Reactions

Classical methods to investigate extraction kinetics, which include a Lewis cell, a single drop method, and a rotating disc method, are not effective to measure the interfacial concentration.¹³ Therefore, a modern experimental method has to be able to determine the interfacial concentration of an extractant or complex as a function of time.

High-Speed Stirring (HSS) Method.^{5,6,14} The HSS method made it possible to measure both an interfacial concentration and an extraction rate for the first time by a simple principle (Fig. 1). When a two-phase system is vigorously stirred in a vessel to generate an extremely expanded interfacial area,

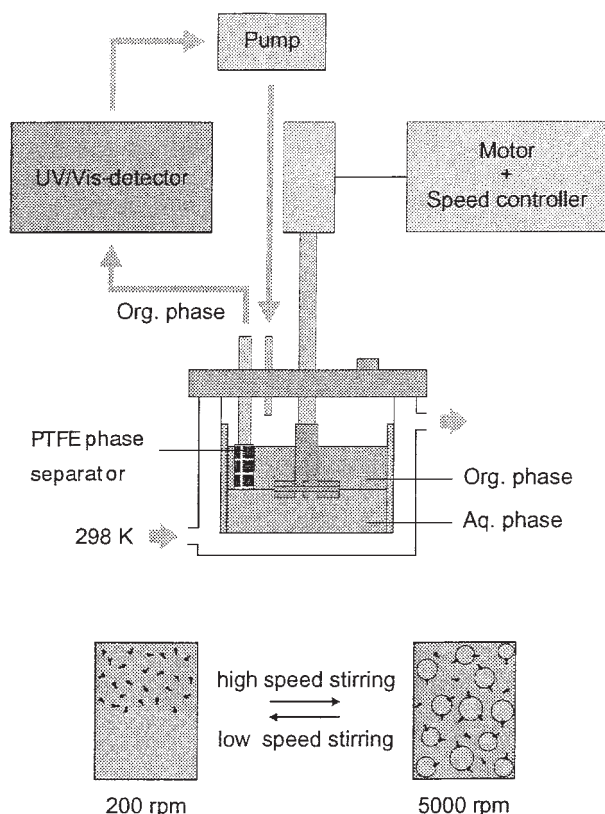


Fig. 1. Schematic drawing of the high-speed stirring (HSS) apparatus. The organic phase was continuously separated by a PTFE phase separator and circulated through the flow cell in the UV/VIS photodiode array spectrometer.

the amount of an adsorbed compound is increased and the concentration in the organic phase is decreased. Therefore, the measurement of the decrease in the organic phase concentration allows one to determine the interfacial amount. Usually, the measurements are carried out by employing 50 mL for each phase and the stirring speed of 5000 rpm. The interfacial area can be increased to 500 times larger than that in a standing condition. The specific interfacial area in HSS condition can become as high as 400 cm^{-1} . The maximum interfacial concentration of an ordinary compound is on the order of $10^{-10} \text{ mol/cm}^2$. This predicts that the maximum amount of an adsorbable solute at the interface corresponds to the amount of solute in 50 mL solution of 10^{-4} M concentration. This concentration is ready to be measured by an ordinary spectroscopic method such as spectrophotometry and fluorometry. In the original HSS method, the concentration depression in the organic phase was measured continuously by spectrophotometry using a PTFE phase separator and a photodiode array spectrometer. A schematic drawing of the apparatus is shown in Fig. 1. From the spectral change caused by stirring, the interfacial amount of a ligand or a complex was observed as a function of time and the extraction rate was determined.

Centrifugal Liquid Membrane (CLM) Method.¹¹ Direct spectroscopic observation of the interface was attained by the centrifugal liquid membrane (CLM) method (Fig. 2). Two phases, each with a volume of about $100 \mu\text{L}$, are introduced into a cylindrical glass cell with a diameter of 19 mm, which

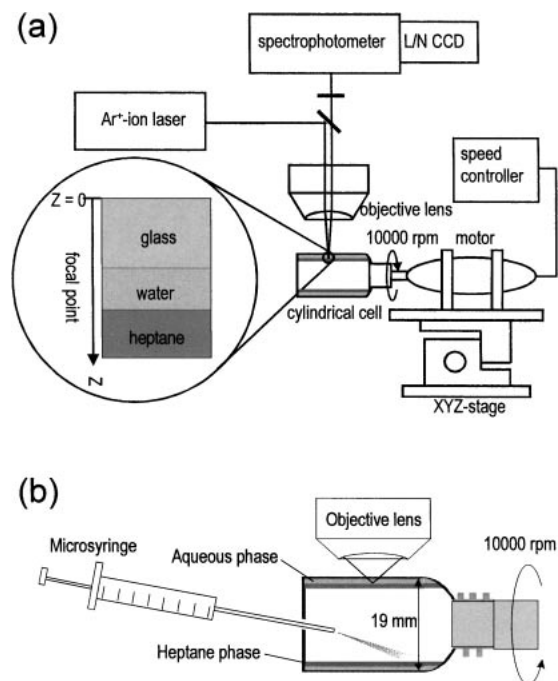


Fig. 2. Schematic drawing of the apparatus for the centrifugal liquid membrane-resonance Raman microprobe spectroscopy (a) and the centrifugal liquid membrane (CLM) cell having a sample injection hole at the bottom (b).

is then rotated at the speed of 10000 rpm. By this procedure, liquid membranes with the thickness of $50\text{--}100 \mu\text{m}$ are produced inside the cell wall, which attains the specific interfacial area of over 100 cm^{-1} . This method can be applied for the measurement of interfacial reaction rates as fast as the order of second.¹¹ The CLM method can be combined with any kind of spectroscopic method. Fluorescence lifetime of an interfacially adsorbed zinc-tetraphenylporphyrin complex was observed by a nanosecond time-resolved laser induced fluorescence method.¹⁶ Microscopic resonance Raman spectrometry was also combined with the CLM (Fig. 2).¹⁷ These combinations were highly advantageous to measure the concentration profiles at the interface and in a bulk phase simultaneously.

Two-Phase Stopped Flow Method.¹⁸ Stopped flow mixing of organic and aqueous phases was an excellent way to produce a dispersion within a few ms. The specific interfacial area of the dispersion became as high as 700 cm^{-1} and the interfacial reaction in the dispersed system could be measured by a conventional photodiode array spectrophotometer. A drawback of this method is the limitation of measurable time. Even in a rather viscous solvent like dodecane, the dispersion system was stable for ca. 200 ms. However, this method is still advantageous for the measurement of fast interfacial reactions such as diffusion limiting reactions as observed in the protonation reaction of tetraphenylporphyrin at dodecane/acid interface.¹⁸

Micro-Two-Phase Sheath Flow Method.¹² The successful measurement of fast interfacial reactions less than 1 ms was accomplished by the micro-two-phase sheath flow method combined with fluorescence microspectroscopy. The schematic drawing of the laser-induced fluorescence measurement in the sheath flow system is shown in Fig. 3. An inner cylindrical

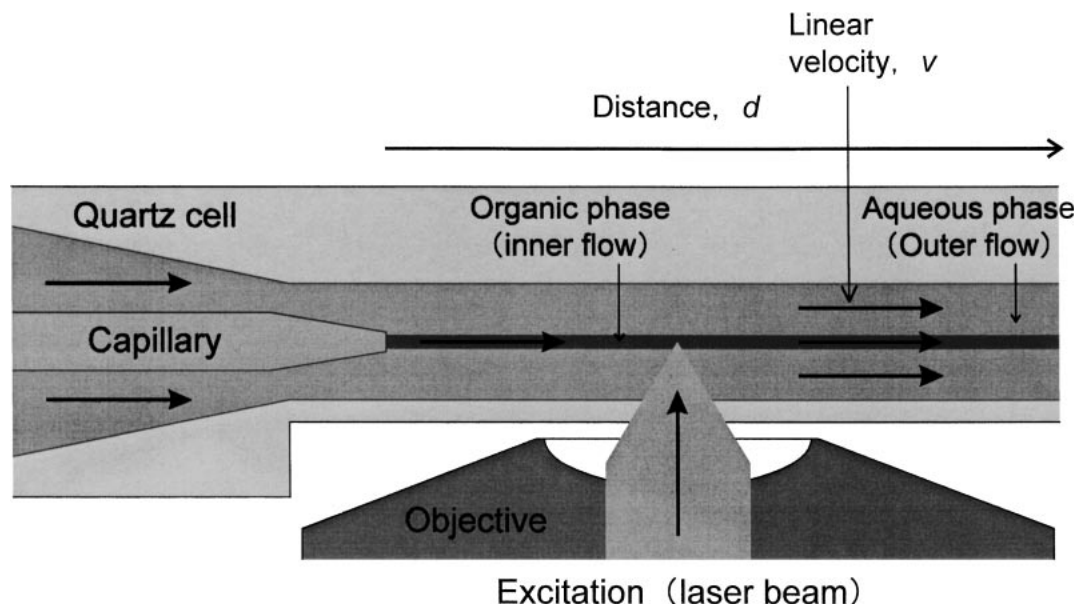


Fig. 3. Schematic drawing of the laser fluorescence microscopy for the measurement of fast interfacial reactions in the micro-two-phase sheath flow systems.

organic phase was flowed with a diameter of 10–30 μm in an aqueous phase flowed with the same linear velocity. The fluorescence spectrum at the interface was observed as a function of the distance from the tip of the inner capillary, which was the start-point of the reaction. The distance from the tip was converted to the reaction time. Then, a very fast interfacial reaction less than 1 ms could be measured by increasing the flow rate. Even a weak fluorescence could be well detected by signal accumulation at a given point. By this technique, it will be possible to detect a fast interfacial reaction of the order of 10 μs . Therefore, this technique is analogous to the continuous-flow method developed for a homogeneous fast reaction.¹⁹

Total Internal Reflection and External Reflection Spectrometry. Total internal reflection (TIR) fluorometry is the most sensitive method for the detection of interfacial species and for the measurement of its dynamics.²⁰ Time-resolved laser spectrofluorometry elucidated the rapid rotational dynamics of a fluorescent dye at the interface.^{21,22} To investigate these rotational dynamics, a time-resolved fluorescence anisotropy was measured using a set of equipment containing a pulsed dye laser (wavelength, 536 nm; pulse width, 0.5–1.0 ns; repetition rate, 10–20 Hz), a streakscope, and a Glan-Thompson analyzer.²³ In a drum-shaped cell, the toluene–water interfacial system was prepared. S- and p-polarized types of laser light were irradiated with an incident angle of 70°, which was larger than the critical angle for the toluene–water interface ($\theta_c = 63^\circ$ at 536 nm).²³

By use of the laser excitation technique, the decay of the triplet state of porphyrin was observed at the interface.²⁴ In the case that an organic phase contains light absorbing compounds, external reflection (ER) absorption spectrometry was more useful than total internal reflection spectrometry.^{25,26} Another advantage of the ER method is that its sensitivity is higher than that of the TIR method, especially for s-polarized light. Therefore, it can be used as a universal absorption spectrometry method of adsorbed species.

Electrochemically Controlled Interfacial TIR Fluorescence and SHG Spectroscopy. The potential modulation spectroscopy, in which the spectroscopic signal is associated with a sinusoidal modulation of the Galvani potential difference ($\Delta_o^w\phi$), allows one to measure the interfacial processes of ions such as ion-transfer and ion-adsorption. The potential modulation spectroscopy has been applied to the interfaces between two immiscible electrolyte solutions (ITIES) in combination with fluorescence^{27–30} and reflectance^{31,32} detections. In particular, potential-modulated fluorescence (PMF) spectroscopy in a total-internal reflection (TIR) condition showed a high selectivity to the interfacial species and the phenomena such as ion-transfer. Considering the dependence of PMF response on the Galvani potential difference and its perturbation frequency, one can analyze the ion-transfer mechanism including interfacial adsorption processes.

The sinusoidal perturbations of the Galvani potential difference is applied as

$$\Delta_o^w\phi = \Delta_o^w\phi_0 + \Delta_o^w\phi_1 \exp(i\omega t) \quad (1)$$

where ω is the angular frequency, i is the imaginary number and the subscripts 0 and 1 correspond to the steady state and frequency-dependent components, respectively. The frequency-dependent fluorescence response (ΔF_t) associated with a quasi-reversible ion transfer can be correlated with the Faradaic ac current ($I_{f,1}$),^{27,33}

$$\Delta F_t = \frac{4.606\epsilon\Phi I_{\text{exc}}}{i\omega|z|F \cos\psi} I_{f,1} \quad (2)$$

where ϵ , Φ , I_{exc} , z , F and ψ are the molar absorptivity, the fluorescence quantum yield, the excitation photon flux, charge number of transferring ion, Faradic constant, and angle of incidence, respectively. The magnitude of $I_{f,1}$ can be estimated from the ion transfer impedance (Z_f),

$$I_{f,1} = \frac{\Delta_o^w \phi_1}{Z_f} = \frac{\Delta_o^w \phi_1}{R_{ct} + (1-i)\sigma\omega^{-0.5}} \quad (3)$$

where R_{ct} and σ are the charge transfer resistance and the Warburg term, respectively. In the case that the adsorption of ionic species is described by the potential-dependent adsorption model based on Langmuir isotherm, the frequency dependent fluorescence response (ΔF_a) associated with adsorption from aqueous phase to the interface can be expressed as a function of ac surface coverage (θ_1):²⁹

$$\Delta F_a = 2.303 \varepsilon \Phi I_{exc} \Gamma_s S \theta_1 \quad (4)$$

where Γ_s is the saturated interfacial concentration and S is the illuminated interfacial area. θ_1 is described as

$$\theta_1 = \frac{bzF\Delta_o^w \phi_1}{RT} \left[\frac{k_{a,0}\alpha c_0(1-\theta_0) - k_{d,0}(\alpha-1)\theta_0}{k_{a,0}c_0 + k_{d,0} + i\omega} \right] \quad (5)$$

where b is the portion of the applied potential employed for adsorption process ($b^w + b^{org} \leq 1$), α is the overall transfer coefficient for adsorption process, c_0 is the bulk concentration, and $k_{a,0}$ and $k_{d,0}$ are adsorption and desorption rate constants at given potentials. The appropriate reverse sign is applied to Eq. 5 for the adsorption process from the organic phase. The potential dependence of the real and imaginary components of ΔF_a for the adsorption from aqueous side exhibits the 180° phase shift to the adsorption from organic side. In the case of a cationic species, the maximum PMF response for the adsorption at the aqueous side appears at potentials less positive than the formal transfer potential $\Delta_o^w \phi^{o'}$ taken as 0 V. In contrast, the PMF response for adsorption at the organic side is maximized at potentials more positive than $\Delta_o^w \phi^{o'}$. The potential dependence of PMF signals is strongly affected by the potential distribution in each phase, i.e. b^w and b^{org} , as well as by the charge number of transferring ion.

Surface second harmonic generation (SSHG) has been applied to investigate the adsorption behavior and physicochemical properties of a variety of surface active species at the interface, such as surface coverage, molecular orientation, and solvation structure.^{34–45} In the case of the adsorption of

non-linear active molecules at the interface, the non-linear response from the solvent can be neglected. Thus, the square root of the SH intensity ($I^{2\omega}$) is directly proportional to the surface concentration of the adsorbed molecules, since the surface susceptibility is a single order function of the number density of the adsorbed molecules and the molecular hyperpolarizability.^{46–48}

Interfacial Electro-Spray Ionization MS Measurement.⁴⁹

Mass spectrometry is the most powerful technique for the identification of the composition and structure of molecules in solution and on surfaces. However, no one has reported any applications of the mass spectrometry to the liquid–liquid interfaces. Recently, the micro-two phase flow system with a high specific interfacial area was directly ionized by an electrospray ionization method and a micro-two phase system including the interface was introduced into the mass spectrometer (Fig. 4). By this method, the species formed at the interface was detected on the mass spectra. Even a highly hydrophobic species, which was insoluble in water, could be fairly well measured by this method.

Single Molecule Probe Method.⁵⁰ The measurement of a single surfactant molecule adsorbed at the interface has been attained by TIR fluorescence microscopy. The observation area at the interface was controlled by a semi-confocal configuration to several hundred nm in diameter. Only fluorescence emitted from the single molecule that entered the observation region at the interface was observed through a microscope with an avalanche photodiode detector. The schematic drawing of the total internal reflection fluorescence microscope for the single molecule detection is shown in Fig. 5. The apparatus consisted of an inverted microscope, an oil immersion objective (PlanApo 60x, NA 1.4, working distance 0.21 mm), a cw-Nd:YAG laser (532 nm), and an avalanche photodiode detector (APD), which provided a quantum efficiency of about 65–67% at 570–600 nm. A pinhole of 50 μm in diameter was attached just in front of the photodiode, which restricted the observation area to 830 nm in diameter (d_{obs}). A laser beam was focused by a lens to the interface through a quartz rectangular prism on a flat two-phase microcell. The shape

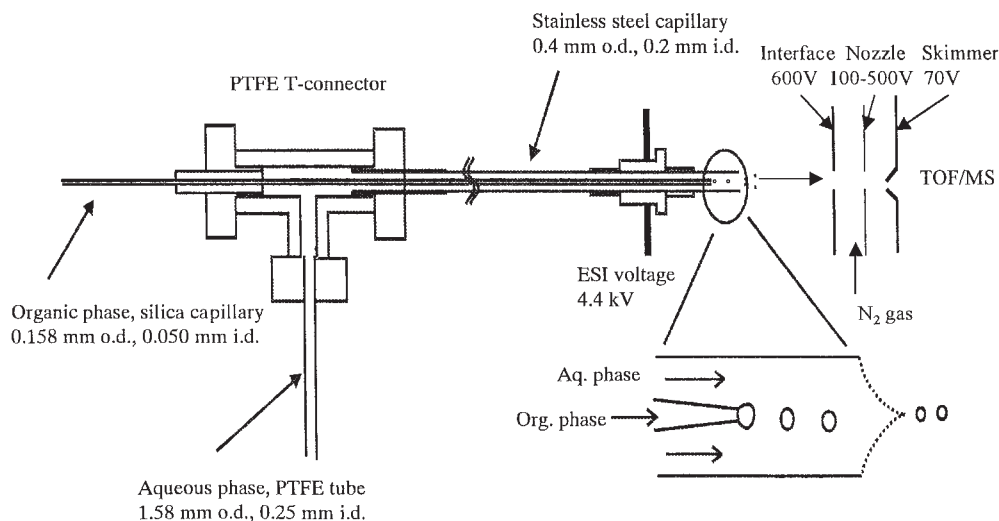


Fig. 4. Direct electro-spray MS method of micro-two phase system. The organic droplet formed at the tip of inner capillary and detached after several seconds was electro-sprayed and introduced into TOF mass or quadrupole mass spectrometer.

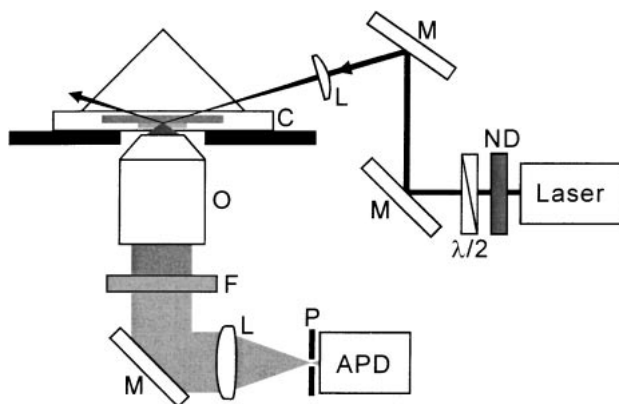
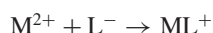


Fig. 5. Schematic illustration of a laser induced fluorescence microscope with the total internal reflection configuration for the detection of single DiI molecules at the dodecane–water interface. Abbreviations: ND, ND filter; $\lambda/2$, $\lambda/2$ plate; M, mirror; L, lens; C, microcell containing dodecane and aqueous phases; O, objective (60 \times); F, band pass filter; P, pinhole; APD, avalanche photodiode detector.

of the laser spot at the interface was an ellipse of about 30 μm \times 100 μm in size. P-polarized laser light was irradiated at an incident angle of 73° at the interface, which was larger than the critical angle. Fluorescence emitted by interfacial molecules was collected by the objective and it was focused on the pinhole after passing through a bandpass filter (path range, 587.5–612.5 nm). Time-resolved photon counting was carried out with a multichannel scalar. The overall detection efficiency of fluorescence at the interface was calculated as 3.3%.

Interfacial Mechanisms in the Extraction of Metal Ions

Chelate Extraction and Interfacial Catalysis. The extraction kinetics of Ni(II) and Zn(II) with *n*-alkyl substituted dithizone (HL) was the first system, in which an interfacial kinetics was elucidated by HSS method.^{3,5,6} The observed extraction rate constants linearly depended on both the metal ion concentration $[\text{M}^{2+}]$ and the hydrogen ion concentration in the aqueous phase. However, the observed extraction rate constant k' was not decreased with the increase of the distribution constant K_D of the ligands, as had been expected from the aqueous phase mechanism. Furthermore, the HSS method revealed that the dissociated form of the *n*-alkyl-dithizone did adsorb at the interface generated by the vigorous stirring.⁵ From these experimental results, the following scheme was proposed by considering both the aqueous phase reaction and the interfacial reaction between M^{2+} and the dissociated form of the ligand L^- :



k , formation rate constant in bulk aqueous phase



k_{i} , interfacial formation rate constant

The rate law for the extraction was obtained as:

$$-\frac{d[\text{M}^{2+}]}{dt} = k' \frac{[\text{M}^{2+}][\text{HL}]_{\text{o}}}{[\text{H}^+]} \quad (6)$$

and the observed extraction rate constant k' was represented by

$$k' = (k + k_{\text{i}}K_{\text{L}}'A_{\text{i}}/V)K_{\text{a}}/K_{\text{D}} \quad (7)$$

where A_{i}/V refers to the specific interfacial area, K_{a} the dissociation constant and K_{L}' the adsorption constant of L^- from the aqueous phase to the interface. Under the conditions of $k \ll k_{\text{i}}K_{\text{L}}'A_{\text{i}}/V$, the above equation is reduced to

$$\log k'K_{\text{D}}/K_{\text{a}} = \log k_{\text{i}} + \log K_{\text{L}}'A_{\text{i}}/V. \quad (8)$$

The value of $K_{\text{L}}'A_{\text{i}}$ was determined by the HSS method. Linear relationships of the above equation were proved experimentally and calculations gave the interfacial rate constants of $\log(k_{\text{i}}/\text{M}^{-1}\text{s}^{-1}) = 8.08$ for Zn^{2+} system and $\log(k_{\text{i}}/\text{M}^{-1}\text{s}^{-1}) = 5.13$ for Ni^{2+} system, respectively.⁵

A primary criteria of the interfacial mechanism is that the ligand concentration dependence of the extraction rate shows a Nernst isotherm or an adsorption isotherm. This was proved in the extraction of Ni(II) with 2-hydroxy oxime such as 5-nonylsalicylaldehyde oxime (P50),⁵¹ 2-hydroxy-5-nonylacetophenone oxime (SME529)⁵² and 2'-hydroxy-5'-nonylbenzophenone oxime (LIX65N).⁵³ These extractants adsorbed at the interface in their neutral forms, obeying the Langmuir isotherm,

$$[\text{HL}]_{\text{i}} = aK'[\text{HL}]_{\text{o}}/(a + K'[\text{HL}]_{\text{o}}) \quad (9)$$

where $[\text{HL}]_{\text{i}}$ and $[\text{HL}]_{\text{o}}$ refer to the concentrations at the interface and the organic phase, respectively; a is the saturated interfacial concentration; and K' is the interfacial adsorption constant defined by $K' = [\text{HL}]_{\text{i}}/[\text{HL}]_{\text{o}}$ under the condition of $[\text{HL}]_{\text{o}} \rightarrow 0$. The interfacial adsorptivity was confirmed also by the interfacial tension measurement. The initial rate constant for the extraction, r^0 , was represented by

$$r^0 = k_{\text{i}}K_{\text{a}}'n_{\text{i}}[\text{Ni}^{2+}]/[\text{H}^+] \quad (10)$$

where K_{a}' is the dissociation constant at the interface and n_{i} is the interfacial amount of the ligand under the present experimental conditions. A linear relationship between r^0 and n_{i} was experimentally confirmed. Then, it was concluded that the reaction between the dissociated form, L^- and the metal ions at the interface governed the extraction rate. The complex formed at the interface was not adsorbed at the interface, but extracted into the organic phase. We determined the adsorption constants of the three 2-hydroxy oximes and the complexation rate constants with Ni(II) and Cu(II) ions at the interface by means of the HSS method as listed in Table 1. The adsorption constants (K') of the neutral forms were all in the order of 10^{-3} cm and the complexation rate constants of the dissociated form with Ni(II) ion at the interface were in the order of $10^5 \text{ M}^{-1}\text{s}^{-1}$ for the three extractants, though the distribution constants (K_{D}) were significantly different. The complexation rate constants were not seriously affected by the interface of heptane/water in comparison with those in bulk aqueous solution. However, in the chloroform system, the magnitude of k_{i} was decreased about two orders. The ligand might be solvated by chloroform molecules even when it was adsorbed.

The adsorptivity of the 2-hydroxy oxime and its orientation at the interface were well depicted by the MD simulations.⁵⁴ It was shown that the polar groups of $-\text{OH}$ and $=\text{N}-\text{OH}$ of the adsorbed 2-hydroxy oxime molecule were accommodated in

Table 1. Kinetic Parameter Obtained in the Adsorption and Extraction of Ni(II) and Cu(II) with 2-Hydroxy Oxime in 0.1 M (H,Na)ClO₄ at 25 °C

2-Hydroxy oxime	pK _a	log K _D (org. solvent)	log a mol cm ⁻²	log A _i cm ²	log K' cm	log k _i M ⁻¹ s ⁻¹
Ni(II)/5-Nonylsalicyl aldehyde oxime(P50)	9.00	3.36 (heptane)	-9.60	4.11	-3.34	4.57
Ni(II)/2'-Hydroxy-5'-nonylacetophenone oxime(SME529)	9.79	3.99 (heptane)	-9.70	4.29	-3.29	5.11
Ni(II)/2-Hydroxy-5-nonylbenzophenone oxime(LIX65N)	8.70	5.69 (heptane) 4.6* (chloroform)	-9.76	4.28	-2.97	5.14
			log a A _i = -6.50 log K' A _i /cm ³ = -0.16			3.33
Cu(II)/LIX65N	8.70	5.69 (heptane)	-9.76	4.28	-2.97	9.87

* Ref. 101.

the aqueous phase so as to react with Ni(II) ion in the aqueous phase.⁵⁵ This was thought to be the reason why the reaction rate constants of Ni(II) at the heptane/water interface had almost the same magnitude as those in aqueous phase. The diffusive and adsorptive behavior of LIX65N around the interface was also simulated for 1 ns. The molecule behaved around the interfacial region, moving between the interface and the heptane phase. Estimated interaction energies of LIX65N with surrounding solvent molecules are plotted in Fig. 6 as a function of the position of the N atom of LIX65N molecule. Figure 6 clearly shows that LIX65N is more stable at the interface than in heptane phase in terms of the interaction energy.

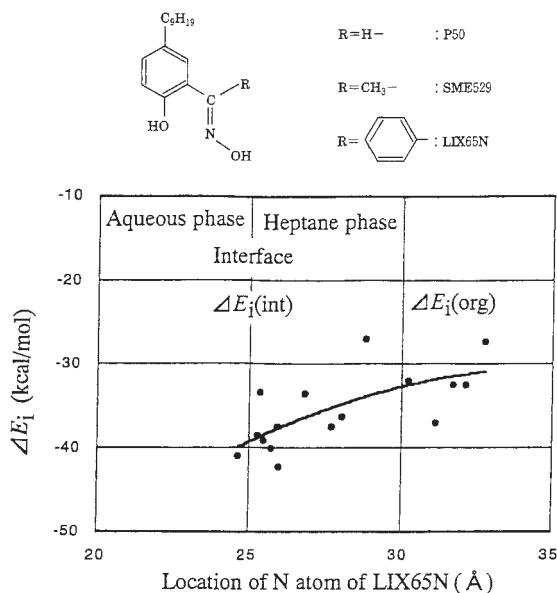


Fig. 6. Structures of 2-hydroxy oxime and the change in the solvation energy with position of the N atom of 2-hydroxy-5-dodecylphenyl oxime (LIX65N) molecule estimated in the heptane/water system by the molecular dynamics simulation for 1 ns. It is noted that the LIX65N molecule is stabilized at the interface during its diffusion between the interface and the bulk heptane phase.

Pyridylazophenol-ligands have been widely used in the extraction photometry of various metal ions. For example, 1-(2-pyridylazo)-2-naphthol (Hpan) is one of the most well known reagents, but it shows a slow extraction rate for some metal ions such as Ni(II) and Pd(II). 2-(5-Bromo-2-pyridylazo)-5-diethylaminophenol (5-Br-PADAP) is more sensitive than Hpan for Cu(II), Ni(II), Co(II), and Zn(II), giving the metal complexes with high molar absorptivities in the order of 10⁵ M⁻¹ cm⁻¹. 5-Br-PADAP showed a significant adsorption at the interface of heptane/water under high-speed stirring conditions (5000 rpm). On the other hand, the adsorptivity at the toluene/water interface was very low. Hpan did not adsorb at the toluene/water interface at all. The adsorption constants of 5-Br-PADAP (HL) at the heptane/water and toluene/water interfaces were obtained as log K' A_i (cm³) = 1.64 and log K' A_i (cm³) = -0.367.¹⁴ The solvent effect on the adsorptivity of the ligand affected directly the interfacial reaction rate. In the heptane system, the Ni(II) complex was not extracted into the heptane phase. On the other hand, in toluene system the complex was extracted very slowly. Recently, the extraction rates of Ni(II) and Zn(II) with 5-Br-PADAP were studied by means of CLM.⁵⁶ Direct observation of the interface by means of CLM method clearly showed the formation of the complex only at the interface of heptane/water systems, as shown in Fig. 7. Based on reaction Scheme 1, the initial formation rate was represented by:

$$r_o = \left\{ k[\text{HL}] \frac{V_a}{V_o} + \left(\frac{k_1 k_2 [\text{HL}]_i}{k_2 + k_{-1} [\text{H}^+]} \right) \frac{A_i}{V_o} \right\} [\text{M}^{2+}] \quad (11)$$

where V_a and V_o refer to the aqueous and organic phase volumes and the definitions of k, k₁, k₂, and k₋₁ are shown in Scheme 1. The complexation proceeded almost completely at the interface. The values of the interfacial complexation rate constants are listed in Table 2. The rate constant of k = 5.3 × 10² M⁻¹ s⁻¹ was determined in the aqueous solution by a stopped-flow spectrometry in the region where the formation rate was independent of pH. The conditional interfacial rate constants represented by k_i = k₁k₂[HL]_i/(k₂ + k₋₁[H⁺]) were larger in the heptane/water interface than the toluene/water interface for both metal ions. The molecular dynamics

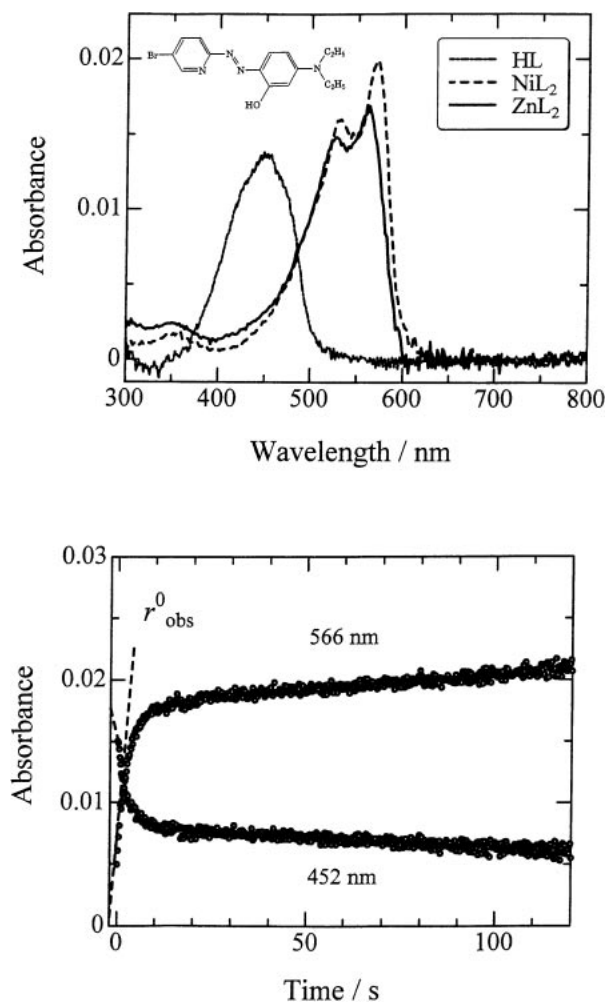
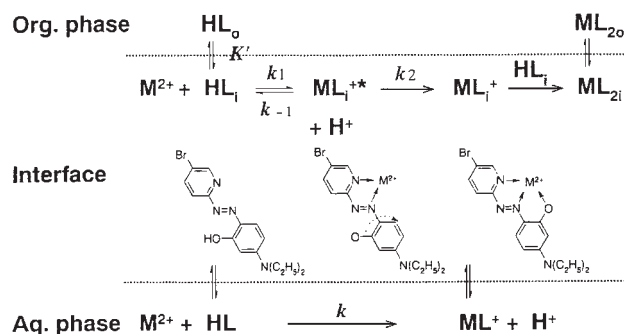


Fig. 7. Absorption spectra of Ni(II) and Zn(II)-5-Br-PADAP complexes at the heptane/water interface (upper) and the formation rate of Zn(II)-5-Br-PADAP complex at the interface measured by the CLM spectrometry (lower). $[HL]_T = 1.5 \times 10^{-5}$ M, $[Zn^{2+}] = 1.0 \times 10^{-4}$ M, pH = 6.0.



simulation of the adsorptivities of 5-Br-PADAP in heptane/water and toluene/water interfaces suggested that 5-Br-PADAP could adsorb at the interfacial region more closely to the aqueous phase, but 5-Br-PADAP in the toluene/water interface was still surrounded by toluene molecules which might lower the probability for it to react with aqueous Ni(II) ions.¹⁴

Table 2. Kinetic Parameters for the Interfacial Complexation of Ni(II) and Zn(II) with 5-Br-PADAP in Heptane/Water and Toluene/Water Systems

Metal ion	$k_1/M^{-1} s^{-1}$	$k_{-1}/M^{-1} s^{-1}$	k_2/s^{-1}
Heptane/water interface			
Ni(II)	1.1×10^3	4.3×10^5	4.4×10^{-2}
Zn(II)	4.4×10^4	6.9×10^5	1.1×10^{-1}
Toluene/water interface			
Ni(II)	3.2×10	2.9×10^4	3.5×10^{-1}
Zn(II)	5.1×10^4	2.0×10^6	4.8×10^{-2}

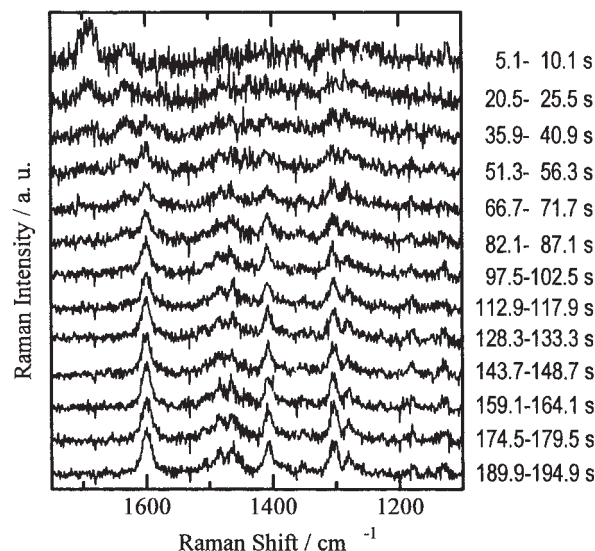


Fig. 8. Change in resonance Raman spectra with the complexation of Pd(II) with 5-Br-PADAP at the heptane-water interface. Aqueous phase: PdCl₂ 8.0×10^{-5} mol dm⁻³, HCl 0.1 mol dm⁻³, pH 1.0; heptane phase: 5-Br-PADAP 7.8×10^{-6} mol dm⁻³. 5-Br-PADAP was injected at 4 s. Final volumes of the aqueous and heptane phase were 0.250 and 0.150 cm³, respectively. Laser power (514.5 nm) was 40 mW and the integration time for each spectrum was 5 s.

We applied CLM-Raman microscope-spectrometry for the measurement of the complexation rate of Pd(II) with 5-Br-PADAP (HL) at the heptane-water interface, and demonstrated that this method was highly useful for the kinetic measurement of the interfacial reaction.⁵⁷ Figure 8 shows a typical result of the spectral change in the interfacial formation of PdLCl. In these Raman spectra, the Raman spectrum of heptane has already been subtracted. Raman intensities at 1599 cm⁻¹, 1408 cm⁻¹, and 1303 cm⁻¹ assigned to PdLCl increased clearly with the reaction time. The initial complexation rate of Pd(II) with 5-Br-PADAP at the interface obtained from the Raman intensity change was in good agreement with that obtained from the absorbance change by CLM spectrophotometry. Furthermore, the resonance-Raman spectra of the interfacial PdLCl provide information on the nano-environment of the complex. Figure 9 shows resonance Raman spectra of PdLCl at the heptane/water and toluene/water interfaces, in toluene, and in ethanol. The resonance Raman spectra of PdLCl adsorbed at the heptane/water and toluene/

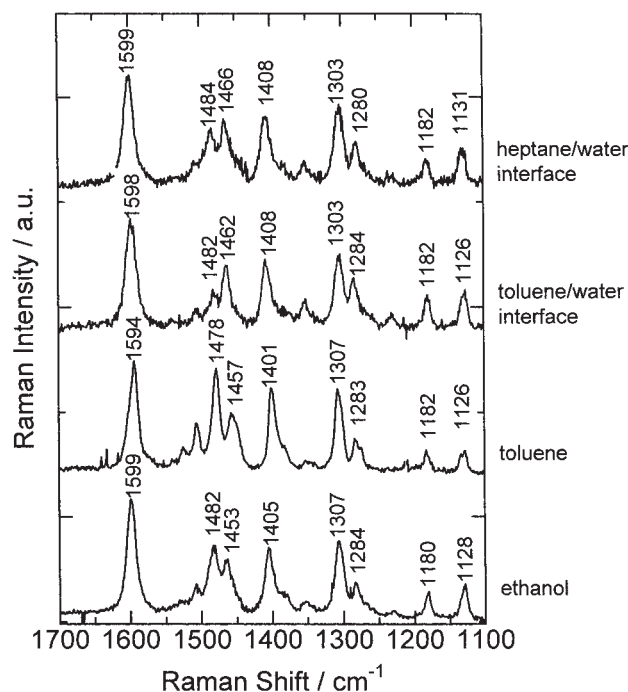


Fig. 9. Resonance Raman spectra of PdLCl adsorbed at the heptane/water and toluene/water interfaces and in toluene and ethanol. Excitation wavelength, laser power, and the integration time were 514.5 nm, 40 mW, and 50 s, respectively.

water interfaces were not in agreement with those in toluene and chloroform of lower dielectric constants, but were close to those in alcohol and aqueous alcohol mixed solvents of higher dielectric constants. This result suggested that the PdLCl complex at the interface was partially surrounded by water molecules. The solvent effect on the resonance Raman spectra of PdLCl reflected the change of the ratio of the azo and imine resonance structures, shown in Scheme 2. The imine contains two forms of imine 1 and imine 2, depending on the extent of the charge separation; imine 1 is more dipolar. The bands at 1482, 1463, 1307, and 1284 cm^{-1} were assigned to $\nu(\text{C}=\text{C})$ of pyridine ring in azo form, $\nu(\text{CNNC})$ in imine form, $\nu(\text{CNNC})$ in azo form, and $\nu(\text{CNNC})$ in imine form, respectively. The azo/imine intensity ratios at 1482 and 1463 cm^{-1} (I_{1482}/I_{1463}) and at 1307 and 1284 cm^{-1} (I_{1307}/I_{1284}) increased with the decrease in the dielectric constant of the solvent. The values of I_{1482}/I_{1463} and I_{1307}/I_{1284} in resonance Raman spectra of PdLCl adsorbed at the toluene/water interface were 0.63 and 1.47, respectively, and those of PdLCl complex formed at the heptane/water interface were 0.86 and 1.85, respectively. From these values, the dielectric constants at the toluene/water and heptane/water interfaces around PdLCl were estimated to be 62 and 40, respectively.

In usual chelate extraction kinetics with an acidic ligand, an acidic condition decreases the extraction rate of metal ions, because of the suppression of the dissociation of the ligand. However, in the extraction of Pd(II) chloride with 5-Br-PADAP in toluene, the lowering of pH accelerated the extraction rate.⁵⁸ The protonation of 5-Br-PADAP at the N_β atom of azo

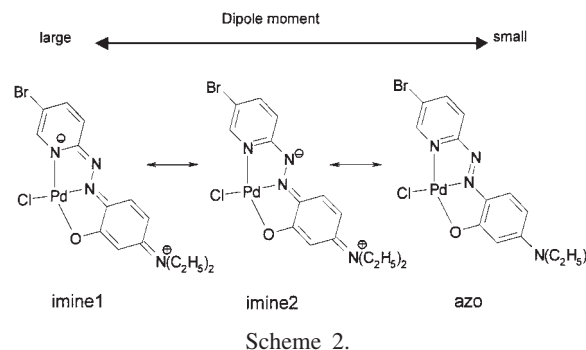


Table 3. The Rate Constants ($\text{M}^{-1} \text{s}^{-1}$) for the Reaction of Pd(II) with the Neutral and the Protonated 5-Br-PADAP in the Aqueous Phase and at the Heptane/Water and Toluene/Water Interfaces

Reaction site	Neutral 5-Br-PADAP (HL)	Protonated 5-Br-PADAP (H_2L^+)
Aqueous phase	5.7×10^2	5.7×10^2
Heptane/water interface	5.3×10	5.1×10^2
Toluene/water interface	6.6×10	3.3×10^2

group increased its adsorptivity at the interface, but did not decrease the reactivity with Pd(II). The rate constants obtained in heptane/water and toluene/water interfaces by CLM method are listed in Table 3.¹⁵ The rate constant is larger for the reaction with the protonated 5-Br-PADAP, because Pd(II) is coordinated by chloride ion and then negatively charged as PdCl_3^- and PdCl_4^{2-} . This type of acid-catalyzed effect has never been reported and is a specific catalysis at the liquid–liquid interface. This finding will provide inspiration for the design of a new type of catalytic extractant that will be interfacially active and strongly reactive for a negatively charged complex ion.

The fast complexation rate between Zn(II) ion with 5-octyloxymethyl-8-quinolinol (Hocqn) at the 1-butanol/water interface was measured by the micro-two-phase sheath flow method.⁵⁹ The formation of a fluorescence complex at the interface was measured in the period less than 5 ms after the contact of the two-phase as shown in Fig. 10(a). The depth profile of the fluorescence intensity through the inner organic flow proved that the fluorescence complex was formed only at the interface in proportional to the time (Fig. 10(b)).

These results showed that the liquid–liquid interface could catalyze the extraction rate by increasing the interfacial concentration of extractant and facilitating the interfacial complexation rate, similar to a gas/solid or a liquid/solid catalysis.

Ion-Association Extraction and Ion-Association Adsorption. Complexes of Fe(II), Cu(II), and Zn(II) with 1,10-phenanthroline (phen) and its hydrophobic derivatives exhibited remarkable interfacial adsorptivity, although the ligands themselves can hardly adsorb at the interface, unless they become protonated.^{60–62} The extraction rate profiles of Fe(II) with phen and its dimethyl (DMP) and diphenyl (DPP) derivatives into chloroform were investigated by the HSS method.⁶³ In the presence of 0.1 M NaClO_4 , both the formation rate of the phen complex and its interfacial adsorption were remarkably dependent on the hydration tendency of anions of Cl^- and

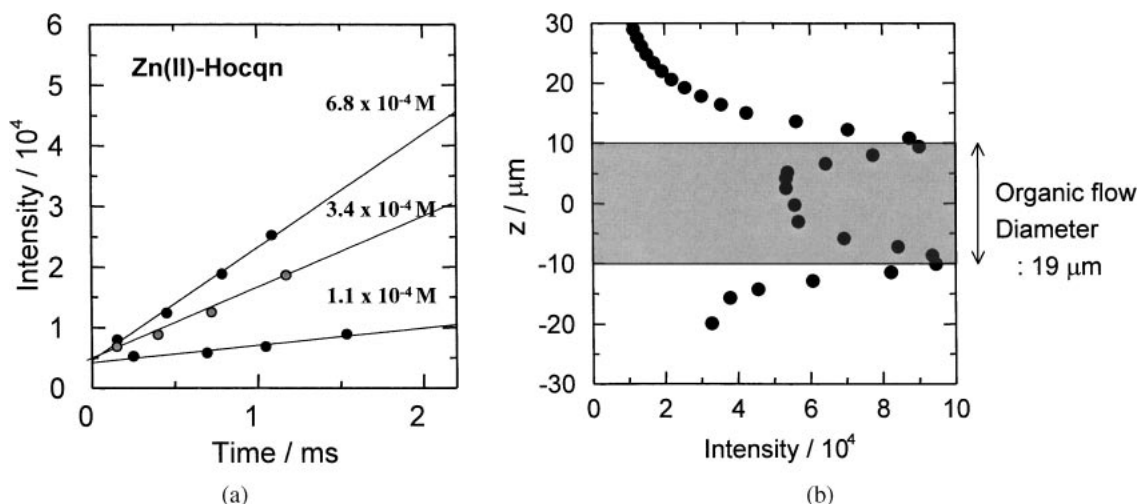


Fig. 10. (a) Formation rate of the fluorescent $\text{Zn}(\text{ocqn})_2$ complex in the 1-butanol/water interface measured by the laser-induced fluorescence measurement for the different Hocqn concentration in $[\text{Zn}^{2+}] = 1.2 \times 10^{-2} \text{ M}$ and $\text{pH} = 6$. (b) Depth profile of the fluorescent $\text{Zn}(\text{II})$ -ocqn complex across the inner 1-butanol phase flow at 1.9 ms after the contact of the two phases. The two peaks correspond to the interfacial region. Conditions are $[\text{Hocqn}] = 1.1 \times 10^{-3} \text{ M}$, $[\text{Zn}^{2+}] = 1.2 \times 10^{-2} \text{ M}$, and $\text{pH} = 6.3$ by MES buffer.

ClO_4^- . The initial extraction rate was described by the equation:

$$\left(\frac{d[\text{FeL}_3\text{X}_2]}{dt}\right)_{t=0} = k_1[\text{Fe}^{2+}][\text{L}] + k_1'[\text{Fe}^{2+}][\text{L}]_i A_i/V_o \quad (12)$$

where k_1 and k_1' stand for the 1:1 formation rate constant of FeL^{2+} in the aqueous phase and at the interface, respectively. The apparent extraction rate constant, k_{obs} , was written as

$$k_{\text{obs}} = \frac{1}{1 + K_C' A_i/V_o} \left(\frac{k_1}{K_D} + k_1' K_L' \frac{A_i}{V_o} \right) \quad (13)$$

where K_L' and K_C' refer to the adsorption constants of L and FeL_3X_2 from organic phase to the interface, respectively. Experimental results showed that the rate-determining step was the 1:1 complex formation both in aqueous phase and at the interface. The adsorption of ligand accelerated the extraction (a positive catalytic effect), but the adsorption of the complex apparently suppressed the extraction rate (a negative catalytic effect). The effects of anion and solvent on the extraction rate could be explained through the change of the adsorption constant K_C' of the tris-complex ion.

Hydrophobic porphyrins of tetraphenylporphyrin (TPP) and octaethylporphyrin (OEP) could be adsorbed at the toluene/sulfuric acid interface by the di-protonation.⁶⁴ On the other hand, the ion-association extraction of the di-protonated porphyrins with chlorinated anions occurred in the order of hydrophobicity: chloride ion < perchlorate ion < trichloroacetate ion.

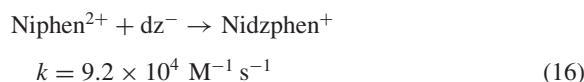
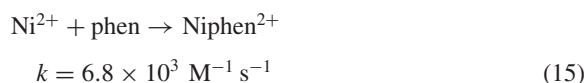
Ion-association adsorption of water soluble porphyrin was studied by TIR fluorometry. Interfacial adsorption of anionic or cationic surfactant succeeded to attract the oppositely charged porphyrin from the mixture of cationic and anionic porphyrins; tetrakis(sulphonatophenyl)porphyrin (TPPS) adsorbed with hexadecyltrimethylammonium ion and tetrakis(*N*-methylpyridyl)porphyrin (TMPyP) with hexadecanesulfonate.⁶⁵ In

addition, the application of an external electric field across the interface controlled the interfacial ion-association adsorption of the ionic porphyrin.⁶⁶ Furthermore, TIR Raman microspectroscopy determined the tilt angle of the orientation of *meso*-tetrakis(*N*-methylpyridyl)porphyrinatomanganese(III) ($\text{Mn}(\text{tmpyp})^{5+}$) with dihexadecyl hydrogenphosphate (DHP) at the toluene/water interface as 65° to the interface normal.⁶⁷

Synergistic Extraction and Interfacial Ligand-Substitution Reaction. A typical kinetic synergism in the extraction of metal ion has been reported for the $\text{Ni}(\text{II})$ -dithizone (Hdz)-phen chloroform system.⁶⁸ The extraction equilibrium constant ($\log K_{\text{ex}}$) was enhanced from -0.7 to 5.3 by the addition of phen:



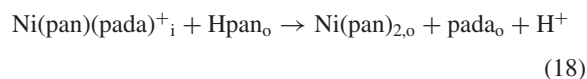
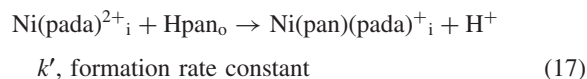
At the same time, the extraction rate was accelerated by the reactions in aqueous phase.⁶⁹ The catalytic effect of phen was explained by the formation of the interfacial adsorptive complex of $\text{Ni}(\text{Dzphen})^+$,



The synergistic effect of DPP on the extraction of $\text{Ni}(\text{II})$ with dithizone was also studied and confirmed the formation of an interfacial complex.⁷⁰

It was suggested that some kinetic synergism could be attained by the formation of an interfacial intermediate complex, which was successively neutralized by a ligand substitution reaction at the interface to form a more extractable, neutral complex. The catalytic effect of *N,N*-dimethyl-4-(2-pyridylazo)aniline (PADA) on the extraction of $\text{Ni}(\text{pan})_2$ was designed along this guiding principle. The extraction rate of

Ni(pan)₂ into toluene was very slow, even under a high-speed stirring condition, whereas the addition of PADA as a low concentration of 10⁻⁵ M could still accelerate the extraction rate about ten times. Into the organic solvent, only Ni(pan)₂ was extracted and no consumption in PADA was observed after the extraction, though a significant decrease in the organic phase concentration of PADA was observed during the extraction under the high-speed stirring condition. These results were analyzed by the mechanism of the interfacial ligand-substitution:⁷¹



The value of k' was obtained as 90 M⁻¹ s⁻¹. The key process of the catalytic extraction of Ni(II)-pan with PADA is the fast aqueous phase formation of Ni(pada)²⁺ and the adsorption of Ni(pan)(pada)⁺ which was followed by the ligand substitution of pada with pan⁻. This scheme has a general importance as a guideline for the acceleration of the extraction rate by the interfacial reaction.

Interfacial Aggregation and Molecular Recognition at the Interface

Another unique feature of the interfacial reaction for metal complexes is the formation of the aggregate of the complex. As observed in many cases, the liquid-liquid interface can be saturated by any surface active molecules at an interfacial concentration of the order of 10⁻¹⁰ mol/cm², which can be attained even under a diluted bulk concentration in the case of highly hydrophobic solutes. This means that the interface is ready to become a two-dimensionally concentrated state for the solute. This situation can very often produce the formation of aggregates of the metal complex at the liquid-liquid interface. During the procedure of solvent extraction of metal ions, we used to encounter the formation of some precipitate at the interface, which is called crud or scum in the field of hydrometallurgy and has to be suppressed. Therefore, this kind of phenomena should be studied more from a viewpoint of an interfacial aggregation of metal complexes.

A typical example of interfacial aggregation is that of the interfacial protonation of tetraphenylporphyrin (TPP). The aggregation rate of H₂tp²⁺ at the dodecane/sulfuric acid solution was measured by a two-phase stopped flow method⁶ and a CLM spectrophotometric method.¹⁰ In the former method, it was found that the stagnant layer of 1.4 μm existed in the dodecane phase side of the droplet interface even under the highly dispersed system. In the CLM method, the liquid membrane phase of 50–100 μm thickness behaved as a stagnant layer where the TPP molecule migrated according to its self-diffusion rate, followed by a rapid protonation and aggregation of the diprotonated species at the interface.

Recently, the formation of the dinuclear Eu(III) complex at the toluene/water interface was determined by time-resolved TIR fluorometry.⁷² When bathophenanthroline sulfate (bps) was added to the extraction system of Eu(III) with 2-thenoyltri-

fluoroacetone (Htta), a double component luminescence decay profile was observed. This indicated the presence of dinuclear complex at the interface.⁷² The observed life times $\tau = 22 \mu\text{s}$ and $203 \mu\text{s}$ were attributed to the dinuclear complex Eu₂(tta)₂(bps)₂ and the mononuclear complex Eu(tta)₂bps⁻, respectively. The shorter life time of the dinuclear complex than $\tau = 98 \mu\text{s}$ for an aqua-Eu(III) ion suggested a charge transfer deactivation in the complex.

Assemblies of Pd(II)-5,10,15,20-tetra(4-pyridyl)porphyrin (tpyp) complex were formed spontaneously at the toluene-water interface, when a toluene solution of tpyp was contacted with an aqueous solution of PdCl₂ under an acidic condition.⁷³ The interfacial assemblies of tpyp were formed with Pd(II) more effectively than with other divalent metal ions: Ni(II), Cu(II), or Zn(II). Pd(II) ion in the complex was bound to the nitrogen of the pyridyl group of tpyp, not to the pyrrole nitrogen. In situ fluorescence microscopy elucidated the formation of two kinds of complex assemblies: assembly 1 (AS1) was generated in a lower tpyp concentration, and assembly 2 (AS2) in a higher tpyp concentration. Steady-state fluorescence excitation and emission spectra were measured under the total internal reflection condition. The fluorescence spectra of interfacial AS2 showed a red-shift of 7–11 nm in the maximum wavelength ($\lambda_{\text{max}} = 668 \text{ nm}$) relative to that of tpyp in toluene, suggesting a weak π -stacking interaction between tpyp molecules in the assembly AS2. Time-resolved TIR fluorometry determined the fluorescence lifetime of AS1 ($\lambda_{\text{max}} = 656 \text{ nm}$) and AS2 as $0.15 \pm 0.05 \text{ ns}$ and $1.1 \pm 0.1 \text{ ns}$, respectively. The average stoichiometric composition of Pd:tpyp was 3:1 and 1:1 for AS1 and AS2, respectively, but the fluorescence quenching effect by Pd(II) indicated that each tpyp of AS1 was bound to four Pd(II) atoms. These results suggested that two Pd(II) atoms in AS1 were shared between two tpyp molecules and that the other two Pd(II) atoms were binding to the nitrogen atoms of the pyridyl group of tpyp molecule as shown in Fig. 11.

We also measured the time-resolved fluorescence anisotropy for the assemblies (AS1 and AS2) of Pd(II)-tpyp complex under the total internal reflection conditions with the incident angle of 70°. ⁷⁴ Since the tpyp molecule could be regarded as a circular light absorber and emitter, the in-plane fluorescence anisotropy (r_Φ) is a function of Θ as well as Φ , resulting in the loss of its intrinsic meaning. Thus, the out-of-plane fluorescence anisotropy ($r_\Theta(t)$) was mainly analyzed in detail. In the case of the tpyp molecule, $r_\Theta(t)$ is written as:

$$r_\Theta(t) = \frac{\langle (1 - 3 \sin^2 \Theta_0)(1 + \sin^2 \Theta(t)) \rangle}{4 \langle 1 + \sin^2 \Theta(t) \rangle} \quad (19)$$

For random distributions of Θ_0 and $\Theta(t)$, $r_\Theta(0)$ and $r_\Theta(t)$ were calculated as -0.29 and -0.25, respectively.

Table 4 summarizes the total interfacial concentration of tpyp and the ratio of AS1 or AS2. The $r_\Theta(t)$ values in the earlier and later time ranges were attributable to AS1 and AS2 at $2.6 \times 10^{-11} \text{ mol cm}^{-2}$, respectively, since the lifetime of AS1 was shorter than that of AS2 as mentioned above. r_Θ was mainly due to AS2 at $1.3 \times 10^{-10} \text{ mol cm}^{-2}$. Table 4 also summarizes r_Θ and Θ_{eq} values for AS1 and AS2. The r_Θ was defined as the average value around Θ , but the Θ values in Table 4 were calculated by assuming that the tpyp mole-

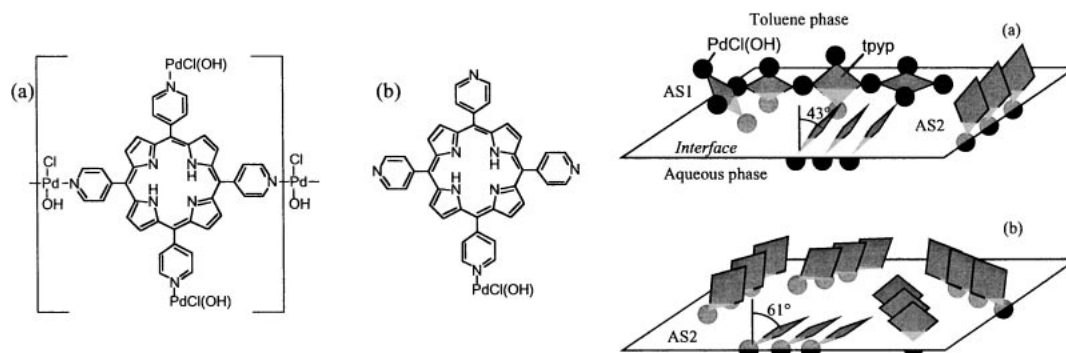


Fig. 11. Schematic illustration of possible structures of the Pd(II)-ttyp complex assemblies at the interface, AS1 and AS2, at the (a) lower and (b) higher total interfacial ttyp concentrations.

Table 4. Out-of-Plane Fluorescence Anisotropy (r_Θ) and Angle Profile as a Function of Interfacial AS1 and AS2 Concentration

	$\Gamma_i^a/\text{mol cm}^{-2}$		
	2.6×10^{-11}	5.4×10^{-11}	1.3×10^{-10}
$[\text{AS1}]/\Gamma_i$	46%	28%	19%
r_Θ for AS1	-0.30	—	—
Θ for AS1	random (or 59°)	—	—
$[\text{AS2}]/\Gamma_i$	54%	72%	81%
r_Θ for AS2	-0.10	-0.17	-0.33
Θ for AS2	43°	49°	61°

a) Total interfacial concentration of ttyp.

cules in AS2 had a fixed Θ_{eq} . Calculations of r_Θ for Θ_{eq} distributions of $43 \pm 10^\circ$ and $61 \pm 10^\circ$ resulted in r_Θ values quite similar to the corresponding ones in Table 4, meaning that the distribution in Θ_{eq} affected the r_Θ values only slightly. As for AS2, Θ_{eq} tended to increase with the increase in the total interfacial ttyp concentration. The function $r_\Theta(r)$ suggested that ttyp in AS1 was randomly oriented. On the other hand, ttyp in AS2 had a halfway orientation angle and it tended to lie at the interface with the increase in its interfacial concentration.

Possible structures of the Pd(II)-ttyp complex assemblies at the interface are schematically illustrated in Fig. 11. Four pyridyl-groups of one ttyp in AS1 were occupied with four Pd(II), two of which bridged two other ttyp molecules. This structure suggests the random distribution of ttyp on the out-of-plane orientation more preferentially than a fixed orientation of 59° . On the other hand, one ttyp molecule in AS2 was bound to one Pd(II) atom. The ttyp molecules in AS2 were weakly associated with each other, and the average aggregation number was about 3. However, it was found that the energy migration between ttyp molecules in AS2 rarely affected on its fluorescence lifetime. In other words, the lifetimes of ttyp in AS1 and AS2 were dominantly determined by the quenching of Pd(II) directly bound to pyridyl-groups. Ttyp in AS2 showed a halfway orientation angle (Θ_{eq}) of about 43° at the lower total interfacial ttyp concentration (2.6×10^{-11} mol cm^{-2}), where the AS1 and AS2 assemblies coexisted at the interface. Ttyp in AS2 tended to lie at the interface ($\Theta_{\text{eq}} \leq 61^\circ$) as the total interfacial ttyp concentration increased to 1.3×10^{-10} mol cm^{-2} , where AS2 assembly was mainly present at the interface.

Isomer-Recognizing Adsorption of Pd(II)-Pyridylazophenol Complex with Diazine Derivative.⁷⁵ Palladium(II) ion can form a 1:1 complex with 5-Br-PADAP, leaving one site for the coordination of another ligand. Pd(II)-5-Br-PADAP (PdL) complex has specific characteristics, such as an extremely high molar absorptivity ($\epsilon_{564} = 4.33 \times 10^4$ M $^{-1}$ cm $^{-1}$ in toluene), an interfacial adsorptivity and a soft Lewis acid. Therefore, PdL can work as an interfacial molecular recognition reagent.

We studied at the start the possibility of molecular recognition of the isomers of diazines by Pd(II)-5-Br-PADAP. Figure 12 shows the molecular structures of the diazines (Dzs or N) studied and their values of the acid-dissociation constant (K_a) and distribution constant between toluene and water (K_D). PdLCl reacted with a neutral Dz and formed a PdL-Dz (PdLN $^+$) complex at the toluene-water interface. The interfacial formation constant (β_i) of PdLN $^+$ complex was defined as:



$$\beta_i = \frac{[\text{PdLN}^+_i][\text{Cl}^-]}{[\text{PdLCl}]_i[\text{N}]} \quad (21)$$

Figure 13 shows the plots of $\log \beta_i$ vs $\log(K_D/K_a)$. The plots were divided into two groups: pyridazine derivatives and the other compounds. A linear relationship was obtained between the logarithmic interfacial formation constants ($\log \beta_i$) for PdL $^+$ -diazine derivative complexes and the logarithmic ratio of the distribution constant (K_D) to the acid-dissociation constant (K_a) for two groups. PdL $^+$ -pyridazine derivative complexes showed much higher stability at the interface than pyrimidine and pyrazine derivative complexes. This result suggests that pyridazine derivative complexes become more liable to adsorb at the interface than pyrimidine and pyrazine derivative complexes, since the bonding of the pyridazine derivative to PdL $^+$ increases its hydrophobicity by the decrease in the dipole moment, which is evaluated by the molecular orbital calculation.

Under the condition of the low concentration of chloride ion, PdL-Dz complexes formed an aggregate at the interface.⁷⁶ Figure 14 shows the absorption spectra of PdLCl and the aggregates of PdL-Dz complexes. The formation of each interfacial aggregate of PdL-Dz was accompanied by a drastic absorbance decrease at 564 nm of PdLCl and changes in the spectral shape. Some differences in the composition of

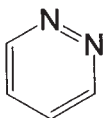
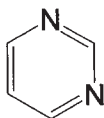
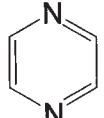
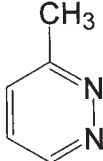
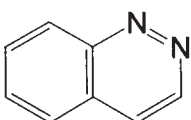
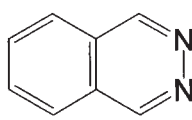
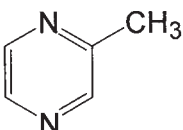
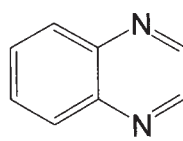
			
1. pyridazine	2. pyrimidine	3. pyrazine	4. 3-methylpyridazine
pK_a 2.30	1.34	0.59	3.24
$\log K_D$ -1.35	-0.540	-0.193	-1.08
			
5. cinnoline	6. phthalazine	7. 2-methylpyrazine	8. quinoxaline
pK_a 2.37	3.50	1.48	0.79
$\log K_D$ 0.597	-0.161	0.188	1.44

Fig. 12. Molecular structures of the diazines (Dzs) studied and their acid-dissociation constants (K_a) and distribution constants (K_D) between toluene and water.

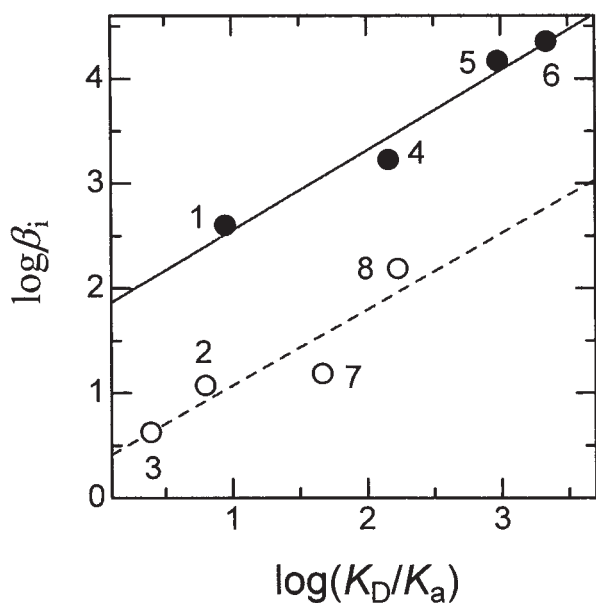


Fig. 13. Linear correlation between the interfacial formation constant ($\log \beta_i$) for PdL^+ -diazine derivative complex in toluene/water and the ratio of the distribution constant to the acid-dissociation constant for diazine derivative ($\log(K_D/K_a)$). Closed and open circles refer to pyridazine derivatives and the other diazine derivatives, respectively. Numbers refer to the diazines in Fig. 12.

the interfacial aggregate of PdL -Dz were observed among Dz isomers; PdL -pyridazine aggregates were blue domains at the interface and the composition ratio was pyridazine: PdL = 1:1, whereas PdL -pyrazine aggregate was as a thin membrane with the composition of pyrazine: PdL = 1:2, and PdL -pyrimidine

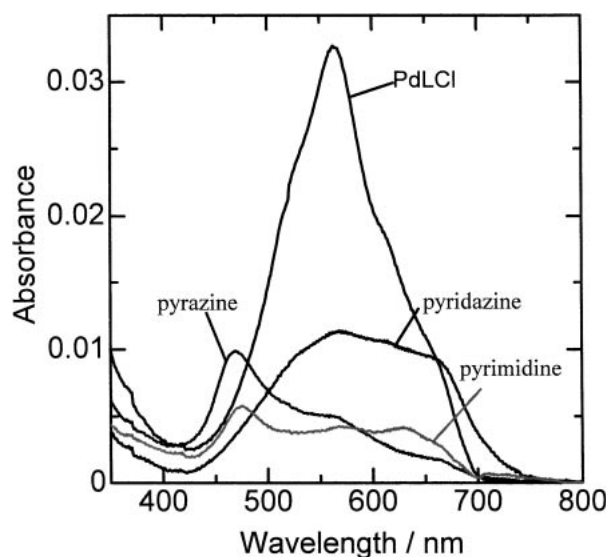


Fig. 14. The absorption spectra of $PdLCl$ and the interfacial aggregates of ternary PdL -Dz complexes measured by CLM method. $[PdLCl]_{init} = 5.6 \times 10^{-5}$ M, $[pyridazine] = 2.0 \times 10^{-4}$ M, $[pyrimidine] = 8.0 \times 10^{-3}$ M, $[pyrazine] = 8.0 \times 10^{-5}$ M, $[ClO_4^-] = 0.1$ M, $[Cl^-] = 0$ M, pH 2.0.

aggregates were blue domains with unknown composition. In spite of the lowest stability for pyrazine among the Dz isomers in the 1:1 complexation with PdL at the toluene-water interface, the stability for the formation of the interfacial aggregate was highest for pyrazine. This result revealed that the formation of the interfacial aggregate of PdL -Dz isomer was governed by the geometric structure of Dz, not by the

basicity. The resonance Raman spectra of the interfacial aggregates measured by the use of the centrifugal liquid membrane method indicated no structural changes of 5-Br-PADAP, such as twisting or *cis*-isomerization.⁷⁷ Moreover, no hypochromic effect in the PdL–Dz aggregates was observed in the aggregate of neutral PdLCl formed at the heptane–water interface. These results suggested that the hypochromic effect in the PdL–Dz complexes resulted from the interaction of 5-Br-PADAP ligand with ClO_4^- as a counter anion incorporated in these aggregates. The interaction should prevent the resonance in the charged quinone structure of the ligand in the Pd(II)–5-Br-PADAP. Similar interfacial aggregation was observed between Pd(II)–5-Br-PADAP and the purine bases, adenine and guanine, of nucleic acid. The interfacial aggregations of PdL with pyridazine, pyrazine, adenine, and guanine occurred at very low concentrations of Dz and purine bases and were not observed in the bulk phases. The interfacial molecular recognizing aggregation found in these systems provided a new mean for the future design of a sensitive and selective detection method for various compounds such as nucleic acid bases, DNAs, drugs and pesticides.⁷⁷

Ion-Adsorption at Electrochemically Polarized Interface

The interfacial adsorption and transfer of ions can be controlled by the application of an electrochemical potential across the interface.^{78,79} The combination of PMF spectroscopy and conventional electrochemical techniques has allowed us to uncover the interfacial adsorption and transfer processes of the fluorescent ions. The supporting electrolytes were bis(triphenylphosphoranylidene)ammonium tetrakis(pentafluorophenyl)borate (BTPPATPFB) for the organic phase and lithium sulfate for the aqueous phase, respectively. The cell was constructed as Ag/AgSO₄/fluorescent ion 0.010 M Li₂SO₄(aq)/0.010 M BTPPATPFB (DCE; 1,2-dichloroethane)/0.001 M BTPPACl, 0.010 M LiCl (aq)/AgCl/Ag.

Tris(2,2'-bipyridyl)ruthenium(II) ($\text{Ru}(\text{bpy})_3^{2+}$) showed quasi-reversible ion transfer features in both these techniques. In this case, the PMF responses for the transfer of $\text{Ru}(\text{bpy})_3^{2+}$ was expressed as a bell-shaped response centered at the formal transfer potential (–0.10 V). On the other hand, the cationic zinc(II) porphyrin, *meso*-tetrakis(*N*-methylpyridyl)porphyrinatozinc(II) ($\text{Zn}(\text{tmpyp})^{4+}$), exhibited rather complex spectroelectrochemical responses, in which the PMF responses indicated that $\text{Zn}(\text{tmpyp})^{4+}$ was adsorbed at the interface at potentials on either side of the formal transfer potential (0.10 V). Due to the difference in the potential dependence of the adsorption processes (Eq. 5), the PMF responses associated with adsorption process from the aqueous phase exhibit a different phase shift with respect to the adsorption from the organic phase. Although the PMF responses for the transfer of $\text{Zn}(\text{tmpyp})^{4+}$ around 0.10 V are superimposed to the adsorption responses, the PMF responses at potentials more negative and positive than the formal transfer potential are related to the adsorption at the aqueous and organic sides, respectively. The PMF signal also indicated that the average orientation of porphyrin ring was close to parallel to the interface.²⁷ The dependence of $\Delta F/F$ on the frequency of potential modulation gave kinetic parameters. The complex representation of PMF responses for the Zn–TMPyP system (Fig. 15)²⁹ measured at the poten-

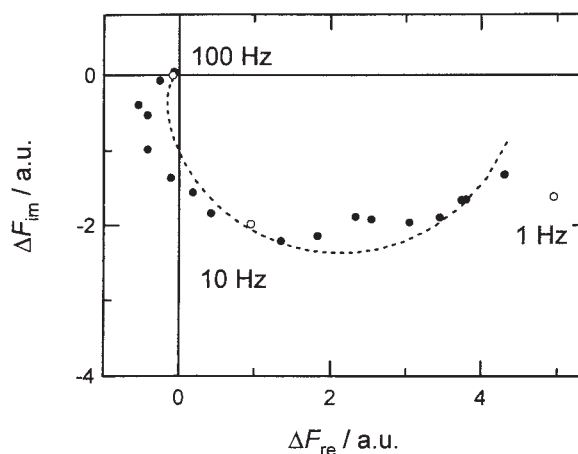


Fig. 15. Complex representation of the PMF responses for the $\text{Zn}(\text{tmpyp})^{4+}$ system at –0.10 V. The concentration of $\text{Zn}(\text{tmpyp})^{4+}$ was 2.5×10^{-5} M. The amplitude of potential modulation was 25 mV. The dashed line was obtained from the curve-fitting with theoretical equations.

tial corresponding to the adsorption process from the aqueous phase, –0.10 V, was expressed by a distorted semicircle, in agreement with the theoretical model for kinetically controlled adsorption processes. In principle, the PMF response is not affected by the non-Faradaic responses such as double layer charging; even so, the spectroscopic responses are still affected by attenuation of the ac-potential due to the uncompensated resistance. The Gibbs free energy of adsorption was evaluated from kinetic parameters as between –30 and –40 kJ mol^{–1}.

Recent surface SHG studies of the adsorption reaction of water-soluble porphyrins at polarized ITIES clearly showed the changes of interfacial species during the ion transfer process via interfacial adsorption.^{80,81} The molecular hyperpolarizability of symmetrically substituted porphyrins has been reported with remarkably small values in the bulk phase, i.e., the order of 10^{–30} esu.^{82,83} These small values for the molecular hyperpolarizability are due to the cancellation of charge transfer interactions along the two dipole moments in the molecule that are intersecting each other. The free base ($\text{H}_2(\text{tmpyp})^{4+}$) and $\text{Zn}(\text{tmpyp})^{4+}$ complex, however, generated intense SHG signals at the water–DCE interface suggesting that the molecular hyperpolarizabilities of these adsorbed molecules were modified at the interface. Figure 16 shows the surface SH spectrum of $\text{H}_2(\text{tmpyp})^{4+}$ at the water–DCE interface. The surface SHG spectrum for the free base was roughly consistent with the bulk absorption spectrum of $\text{H}_2(\text{tmpyp})^{4+}$ in the aqueous solution, suggesting that the electronic structure of the interfacial species is only slightly modified as compared to the bulk species. This emphasizes the high sensitivity of surface SHG to a weak electronic change in a molecule like charge redistribution. No dependence of the molecular orientation of $\text{H}_2(\text{tmpyp})^{4+}$ on the bulk concentration was observed by polarization measurements of SHG intensity, in which the average angle of the rotation axis of D_{2h} symmetry of molecule was obtained as $41 \pm 6^\circ$ with respect to the normal to the interface. The Gibbs free energy of adsorption was estimated as -29 ± 1 kJ mol^{–1} by analyzing the adsorption isotherm. Surface SHG under the electrochemical control

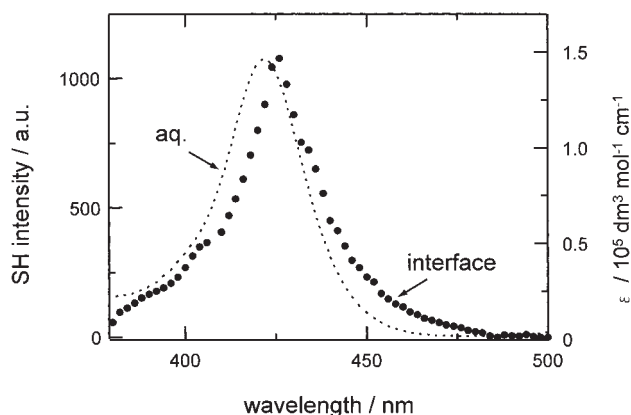


Fig. 16. Surface SH spectrum of $\text{H}_2(\text{tmpyp})^{4+}$ at the water-DCE interface. The concentration of $\text{H}_2(\text{tmpyp})^{4+}$ was 1.0×10^{-5} M. The dashed line relates to the absorption spectra of $\text{H}_2(\text{tmpyp})^{4+}$ in the aqueous phase.

was coupled with the conventional cyclic voltammetry and utilized to evaluate the dependence of adsorption behavior on the Galvani potential difference. The composition of the electrochemical cell was an analogue of the PMF measurements. The adsorption of $\text{H}_2(\text{tmpyp})^{4+}$ prior to the transfer was clearly observed, but it should be noted that the surface SH spectrum remained unchanged within the examined potential range. The increase of the SH intensity at 428 nm was observed at potentials more negative than $\Delta_o^w \phi'$ at 0.02 V and the maximum of the SH intensity was observed around -0.08 V. By applying more positive potentials, the interfacial concentration of $\text{H}_2(\text{tmpyp})^{4+}$ was decreased through the ion transfer into the organic phase.

Similar potential dependence of SH intensity was measured for the anionic water-soluble porphyrin, *meso*-tetrakis(4-carboxyphenyl)porphyrinatozinc(II) ($\text{Zn}(\text{tppc})^{4-}$).⁸⁰ In the Zn-TPPC system, however, significant changes of the interfacial species was observed in comparison with the bulk species. The maximum of surface SH spectrum for $\text{Zn}(\text{tppc})^{4-}$ at the water-DCE interface was observed at 450 nm without electrochemical controls, red-shifted from the absorption spectra of Zn-TPPC, whose absorption maxima were 422.5 nm for the aqueous and 423.5 nm for the organic phases, respectively. Therefore, the species at longer wavelengths was measured only at the interface. A weak SH response was also obtained around 423 nm and this response could be generated from the species, similar to the bulk condition. A red-shift of the Soret band was often observed as the *J*-aggregation took place.^{11,16,43} The SH intensity at 423 nm considered as the response of the non-aggregated form was much smaller than the red-shifted one at all concentrations without applying potentials.

Under the potentiostatic condition, the SH responses of Zn-TPPC exhibited considerable spectral changes. Figure 17(a) shows the potential dependence of the SH intensities measured at 420 nm and 460 nm. The Galvani potential difference was swept from 0.05 V, where Zn-TPPC was initially located in the aqueous phase, to more negative potentials down to -0.35 V and then swept back to the initial potential. The SH signal at 420 nm related to the non-aggregated form in-

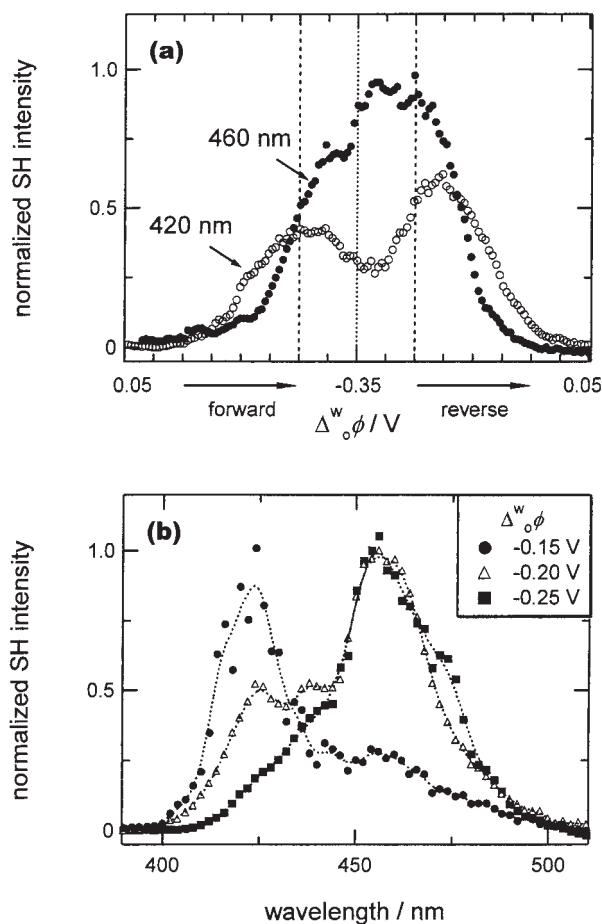


Fig. 17. (a) Potential dependence of SH intensities at 420 nm (hollow circles) and 460 nm (filled circles). The dashed lines refer to the formal ion transfer potential of $\text{Zn}(\text{tppc})^{4-}$ at -0.25 V. (b) Surface SH spectra observed at various applied potentials. The concentration of Zn-TPPC in the aqueous phase was 5.0×10^{-6} M.

creased with the forward potential sweep down to the formal ion transfer potential at ca. -0.25 V. As the porphyrin molecule transfers to the organic phase, the SH signal drops, indicating that the interfacial concentration decreases. On the other hand, the SH signal measured at 460 nm showed a drastic increase delayed from the response at 420 nm, suggesting that the aggregation of Zn-TPPC is eventually taking place after increasing the interfacial concentration of the non-aggregated form. The dependence of the interfacial concentration on the Galvani potential difference was also confirmed by measuring the electrocapillary curves. The surface SH spectrum measured under potentiostatic conditions clearly demonstrated a development of the aggregation by applying more negative potentials (Fig. 17(b)). At -0.15 V, the SH spectrum showed the maximum response around 420 nm, which was related to the non-aggregated form. Applying more negative potentials, one finds that the SH intensity around 420 nm was gradually decreased; an increase of the red-shifted peak was observed around 460 nm. These results indicate that both the concentration and the species at the interface can effectively be controlled by the electrochemical potential.

Relaxation Dynamics at Liquid–Liquid Interfaces

Rotational Dynamics of *N*-octadecylrhodamine B. The adsorption equilibria of fluorescent *N*-octadecylrhodamine B ($C_{18}RB$) at a free toluene–water interface has been clarified by the steady-state total internal reflection fluorometry.²⁰ Both the zwitter ion ($C_{18}RB^\pm$) form and the protonated form ($C_{18}RBH^+$) are fluorescent; they are present only at the interface, whereas the non-fluorescent lactone form ($C_{18}RB^0$) exists only in the toluene phase. There are no species of $C_{18}RB$ in the aqueous phase.

We employed three surfactants: that is, Triton X-100 (TX-100), sodium dodecyl sulfate (SDS), and dihexadecyl hydrogenphosphate (DHP, $pK_a \approx 2$). TX-100 had slight attractive interactions with $C_{18}RBH^+$ at the toluene–water interface at pH 1.0, because TX-100 is nonionic. SDS and deprotonated DHP had attractive interactions with $C_{18}RBH^+$ at the interface at pH 1.0 and 3.0, respectively, due to the electrostatic interaction of the positive $C_{18}RBH^+$ and the anionic surfactants. For all of the three surfactants, the interfacial concentration of $C_{18}RBH^+$ tended to decrease with an increase in the surfactant concentration in the bulk in the range $>10^{-6}$ mol dm⁻³.

We will discuss here about in-plane and out-of-plane rotational dynamics of $C_{18}RB$ at the interface. $C_{18}RB^0$ and DHP were dissolved in toluene, whereas TX-100 and SDS were dissolved in water. S- and p-polarized laser lights were irradiated with an incident angle of 70°, which was larger than the critical angle for the toluene–water interface ($\theta_c = 63^\circ$ at 536 nm).²¹ It is known that the transition dipole moment for the absorption of rhodamine B (RB) at about 530 nm ($S_0 \rightarrow S_1$) is almost parallel to that for the emission at about 570 nm ($S_1 \rightarrow S_0$),¹⁹ and this is applicable to the $C_{18}RB$ molecule.

The definition of coordination axes is displayed in Fig. 18. Time-resolved in-plane fluorescence anisotropy ($r_\Phi(t)$) is obtained as:

$$r_\Phi(t) \equiv \frac{I_{ss}(t) - I_{sp}(t)}{I_{ss}(t) + I_{sp}(t)} = 4(\cos^2 \Phi_a(0) \cos^2 \Phi_e(t)) - 1 \quad (22)$$

where $I(t)$ is a time-resolved fluorescence intensity. The first subscript s corresponds to the excitation with s-polarized light, and the second subscripts s and p mean the detection of s(y)-

and p(x)-polarized types of emission light, respectively. Φ is the angle defined as Fig. 18(a), and subscripts a and e are absorption and emission transition dipole moments, respectively. $\langle \rangle$ is the average for all molecules and over the whole Φ angle range. When the in-plane rotation is restricted in the range of $\Phi_a(0) \pm \Phi_t$ ($0 \leq \Phi_t \leq \pi/2$),

$$r_\Phi(\infty) = 0.5 \frac{\sin(2\Phi_t)}{2\Phi_t} \quad (23)$$

When molecules rotate with a rotational correlation time (τ ; τ_Φ or τ_Θ), $r(t)$ of the molecules can be expressed as:

$$r(t) = \{r(0) - r(\infty)\}e^{-t/\tau} + r(\infty) \quad (24)$$

The intrinsic time constant for the rotational relaxation of $C_{18}RBH^+$ at the interface is faster than 1 ns. This rapid orientation dynamics without restriction was also reported for acridine orange at alkane–water interfaces.⁸⁴

The value of $r_\Phi(t)$ in the 2.5×10^{-8} mol dm⁻³ TX-100 system was 0.16 at $t = 0$; it rapidly decayed to almost 0.1. The apparent τ_Φ value was obtained as 0.9 ns, which was comparable to that in the free system, whereas the $r_\Phi(t)$ value at $t \geq 3$ ns was not 0 but 0.1. At the other TX-100 concentrations, the apparent τ_Φ values were comparable to the pulse width, but the $r(\infty)$ values were not 0. These results indicate that the in-plane rotation of $C_{18}RBH^+$ is not retarded by the interfacial TX-100 molecules. The $r_\Phi(\infty)$ value tended to increase with the increase in the TX-100 concentration, as shown in Fig. 19.

The observed τ_Φ values are larger than the pulse width in the DHP system, indicating that they can be regarded as intrinsic τ_Φ values. Similar relations were obtained in the SDS system, and the observed values are summarized in Table 5. The increase in the τ_Φ values with the increase in the concentration of the anionic surfactant (SDS, DHP) implied that the in-plane rotational relaxation of $C_{18}RBH^+$ was slowed down by the anionic surfactants. It was reported that the fluorescence lifetime of acridine orange in a SDS aqueous solution became longer and the orientational dynamics was retarded due to the formation of aggregate.⁸⁵ However, the fluorescence lifetime of $C_{18}RBH^+$ was almost independent of the surfactant concentration.

Time-resolved out-of-plane fluorescence anisotropy ($r_\Theta(t)$) is obtained as:

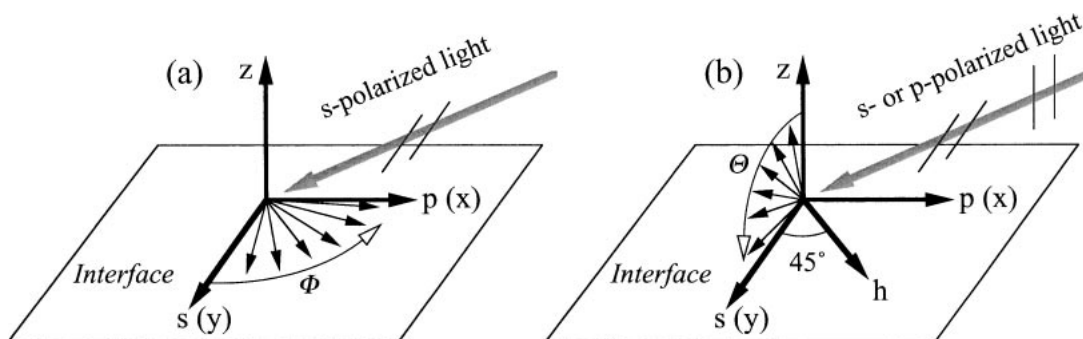


Fig. 18. Cartesian coordination axis (x, y, z) at the toluene–water interface. (a) In-plane fluorescence anisotropy. S-polarized laser lights were irradiated to the toluene–water interface. P(x)-polarized and s(y)-polarized emissions were observed as a function of time. Φ is the angle between the transition dipole moment for emission and y-axis. (b) Out-of-plane fluorescence anisotropy. S- and p-polarized laser lights were irradiated to the toluene–water interface. Fluorescence was observed at h(45°)-axis as a function of time. Θ is the angle between the transition dipole moment for emission and z-axis.

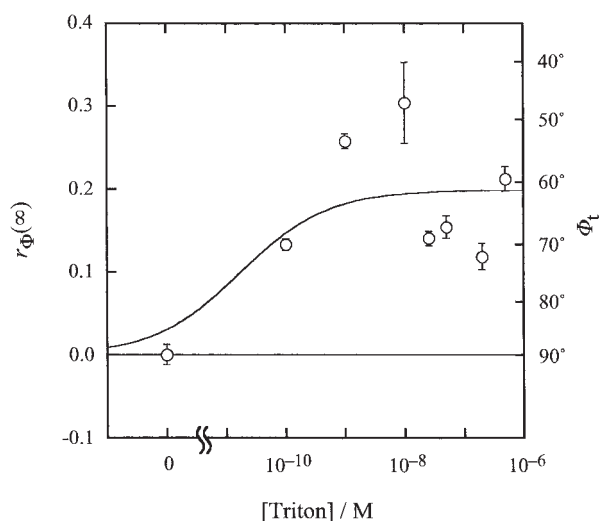


Fig. 19. $r_{\Phi}(\infty)$ as a function of the TX-100 concentration. The line was drawn for the aid of eyes.

Table 5. Evaluation of the Viscosity (η) and the Interfacial Two-Dimensional Viscosity (η_i) at the Toluene/Water Interface

Surfactant	[S]/M	τ_{Φ} /ns	η /Pa s	η_i /Pa m s
—	—	$1.1 \pm 0.2^a)$	$< 3 \times 10^{-3b)}$	$< 8 \times 10^{-13b)}$
TX-100	2.5×10^{-8}	$0.9 \pm 0.1^a)$	$< 3 \times 10^{-3b)}$	$< 8 \times 10^{-13b)}$
SDS	1.0×10^{-7}	$0.9 \pm 0.2^a)$	$< 3 \times 10^{-3b)}$	$< 8 \times 10^{-13b)}$
SDS	1.0×10^{-6}	5.2 ± 1.4	0.023	4.6×10^{-12}
DHP	1.0×10^{-7}	2.7 ± 0.2	0.012	2.4×10^{-12}
DHP	1.0×10^{-6}	21 ± 5	0.091	1.8×10^{-11}

a) Values are comparable to the pulse width of laser, and therefore these are apparent values. b) Only the upper limits for η and η_i could be evaluated.

$$r_{\Theta}(t) \equiv \frac{I_{ph}(t) - I_{sh}(t)}{I_{ph}(t) + 2I_{sh}(t)} \quad (25)$$

$$= 1.5(\cos^2 \Theta_a(0) \sin^2 \Theta_c(t)) / (\sin^2 \Theta_c(t)) - 0.5$$

where the first subscript p means the excitation with a p-polarized light, the second subscript h the detection at an angle of 45° from the y-axis, and Θ is defined as shown in Fig. 18(b). When the molecules are tilted at Θ_{eq} , $r_{\Theta}(0) = r_{\Theta}(\infty) = 1.5 \cos^2 \Theta_{eq} - 0.5$.

Regardless of the surfactants, $r_{\Theta}(t)$ values were independent of time, showing the constant value of -0.23 . This means that the $C_{18}RBH^+$ molecules are tilted at an angle (Θ_{eq}) at the toluene–water interface. The $r_{\Theta}(t)$ values were averaged in the time range of 0–10 ns in each system. The calculated Θ_{eq} values are in the range of $65 \pm 2^\circ$, showing a slight effect of the surfactants. The xanthene ring of $C_{18}RBH^+$ would be tilted by this angle from the normal to the interface.

The in-plane rotational correlation time (τ_{Φ}) obtained in the SDS and DHP systems may be reflected by interfacial characteristics. In a bulk solution, the rotational correlation time (τ) of a fluorophore is expressed as:

$$\tau = \frac{v\eta}{k_B T} \quad (26)$$

where η is the viscosity of the solvent, k_B is the Boltzmann constant, T is absolute temperature, and v is the molecular volume of the solute. The molecular volume of $C_{18}RB$ was estimated to be $9.5 \times 10^{-28} \text{ m}^3$.²¹ The viscosity for water and toluene were 8.90×10^{-4} and $5.53 \times 10^{-4} \text{ Pa s}$ at 25°C , respectively, and τ values of $C_{18}RB$ in these solvents could be calculated as 0.21 and 0.13 ns, respectively. These values were consistent with the experimental results. Therefore, it can be concluded that there is no specific structure at the toluene–water interface, since the τ_{Φ} value is comparable to the value in each bulk solvent, that is, less than 0.5 ns.

The η values in the SDS and DHP systems, which were calculated with Eq. 26 and are listed in Table 5, are clearly higher than those of toluene and water, but are lower than that of glycerol (0.945 Pa s), one of the viscous solvents. The high viscosity of monolayer was also reported at the DHP or mono-alkyl dihydrogenphosphate micelle surface at about pH 5,^{86,87} in which hydrogen-bonding structure was suggested between protonated and deprotonated phosphate.⁸⁸

The two-dimensional interfacial viscosity (η_i ; in Pa m s) was approximately calculated by:²¹

$$\tau_{\Phi} \approx \frac{4\pi\eta_i l^2}{k_B T} \quad (27)$$

where l is the radius of the solute molecule. By assuming the $C_{18}RB$ molecule to be a sphere, its radius could be estimated as $6.1 \times 10^{-10} \text{ m}$. Petkov et al. reported the shear viscosity for air–0.04 M SDS aqueous solution as $1.45 \times 10^{-6} \text{ Pa m s}$ by the measurement for the translational movement of microparticles on the surface,⁸⁹ which was 10^5 – 10^6 times larger than our results. This would be caused by the much higher concentration of SDS than in our case, as well as the difference in the observing site (interface or surface). The fluorescent molecule $C_{18}RBH^+$ is considered to be an alternative probe to evaluate the two-dimensional interfacial viscosity besides microparticles (size, about 0.5 μm) or rotating disks (radius, several ten μm), which were used to measure the shear viscosity of the surface.^{88,89} In comparison with the microparticles, the molecular probe has definite advantages in that the interference of the bulk viscosity is negligibly small and that information about the nano-environment around the probe can be obtained.

The interaction between $C_{18}RBH^+$ and DHP molecules at the toluene–water interface is schematically shown in Fig. 20. The xanthene ring was tilted by $65 \pm 2^\circ$ from the normal to the interface. There is electrostatic attractive interaction between $C_{18}RBH^+$ and anionic surfactant, DHP, at the interface. The in-plane rotational relaxation was affected by the viscosity of the interface.

Relaxation Kinetics of the Excited Porphyrin. Tetra(*N*-methylpyridinium-4-yl)porphyrin (tmpy^{4+}) was adsorbed on a toluene–water interface with dodecyl sulfate ions. The relaxation kinetics for triplet tmpy^{4+} at the interface was measured with probe white light (xenon lamp) and pulsed 532 nm laser light (Nd:YAG; pulse width, 6 ns; 10 Hz) at an incident angle of 67° .²⁴ Triplet tmpy^{4+} was quenched by dissolved oxygen molecule (O_2) under aerated conditions, and $1.84 \pm 0.02 \mu\text{s}$ was obtained as a quenching time constant. The triplet tmpy^{4+} at the interface was quenched faster than in aqueous

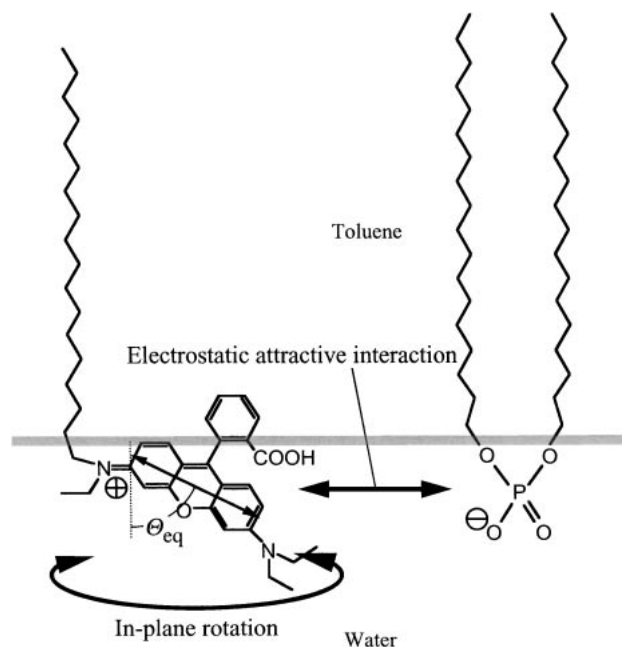


Fig. 20. A probable orientation for the adsorption of $C_{18}RBH^+$ at the toluene–water interface. The xanthene ring is tilted by $\theta_{eq} = 65 \pm 2^\circ$ from the normal to the interface. There is electrostatic attractive interaction between $C_{18}RBH^+$ and anionic surfactant, DHP, at the interface. The in-plane rotational relaxation is affected by the interfacial viscosity.

solutions; $0.72 \pm 0.12 \mu s$ was obtained as a time constant. The faster decay rate at the interface suggested the triplet-triplet annihilation at the interface, because of the increase of the interfacial concentration of tmpyp $^{4+}$.

Dispersion of toluene solution of tetraphenylporphyrin (tpp) in aqueous 2–9 M H_2SO_4 solutions as droplets produced the diprotonated species of tpp (H_2tpp^{2+}) at the toluene–aqueous H_2SO_4 interfaces.⁹⁰ The triplet state of H_2tpp^{2+} generated at the interface by the irradiation of the pulsed laser light of 532 nm was quenched mainly by O_2 . The apparent quenching rate was proportional to the O_2 concentration of the aqueous H_2SO_4 solution, meaning that O_2 in the toluene was not effective for the quenching. Triplet tpp generated in the toluene droplets was normally quenched by dissolved oxygen in the toluene droplets. The concentration of dissolved oxygen in toluene droplets was much higher than the aqueous solutions, but O_2 in toluene was not effective for the quenching of triplet H_2tpp^{2+} at the interface. These facts suggested that H_2tpp^{2+} existed in the aqueous side of the interface. The quenching rate constant at the interface was almost equal to the constants in some organic bulk solutions, suggesting the same quenching process, that is, the formation of a singlet encounter complex, $^1(T_1 \cdot ^3O_2)^*$.

Single Molecule Dynamics at the Liquid–Liquid Interface

A single molecule will be an ultimate probe to measure the properties of the nano-environment of a liquid–liquid interface. Some techniques for the detection of single molecules have been developed; most of them are utilizing laser-induced fluorescence microscopy. Many studies on single molecule

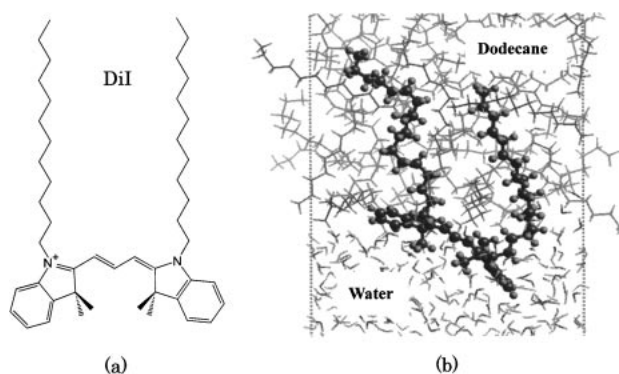


Fig. 21. (a) Chemical structure of DiI, which has two long alkyl-chains and one positive charge. (b) A snap shot of the molecular dynamics simulation of DiI at the interfacial region of dodecane/water system. Each phase has a volume of $(2.5 \text{ nm})^3$ in the simulation.

detection in solutions^{91–94} and at solid–liquid interfaces^{95–97} have been reported, but there are no studies on the single molecule detection at the liquid–liquid interface so far except ours.^{50,98} We demonstrated by using a fluorescent dye that the single-molecule-probing of the interface was a powerful means to evaluate the nano-properties of the interfacial region.⁵⁰ The influence of two kinds of surfactants, that is, sodium dodecyl sulfate (SDS) and dimyristoyl phosphatidylcholine (DMPC), on the lateral diffusion dynamics of single molecules at the interface was also investigated.

As a probe fluorescent molecule, 1,1'-dioctadecyl-3,3,3',3'-tetramethylindocarbocyanine (DiI, Fig. 21) was employed. It is a monovalent cation possessing two C_{18} alkyl-chains, and thus it was adsorbed substantially at the dodecane–water interface. All of the DiI molecules were adsorbed at the interface from the dodecane phase at the initial DiI concentration lower than $2 \times 10^{-7} \text{ M}$. The fluorescence of the interfacial DiI was observed in the range of 571–575 nm.

A two-phase microcell, shown in Fig. 5, was fabricated by sticking a bored (hole 10 mm in diameter) slideglass, a bored (hole 5 mm in diameter) coverslip (0.14 mm in thickness), and another non-bored coverslip in this order. Pure water (2.7 mm^3) filled the lower thin container of the cell in the surfactant-free system. An aqueous solution of SDS filled it in the SDS system. In both cases, a dodecane solution of DiI (63 mm^3) was added on the aqueous layer. A new coverslip was put on the dodecane phase to close the cell.

DMPC was dissolved in chloroform, and the solution was mixed with pure diethyl ether at a ratio of 1:19 (chloroform: diethyl ether) by volume. Pure water was filled in the lower container, and then the DMPC solution (5 mm^3) was quietly spread on the water. After evaporation of chloroform and diethyl ether, the dodecane solution of DiI was added on the DMPC layer. Since DiI had a high adsorptivity to the interface, no DiI molecules remained in the dodecane phase in the initial DiI concentrations lower than $1 \times 10^{-7} \text{ M}$. The contribution of the photobleaching of interfacial DiI was found to be negligibly small in the present study.

The average period (τ_d) that one DiI molecule took to emit one photon was expressed with some kinetic constants and quantum yields concerning the light absorption and emission,

and the intersystem crossing processes of DiI were considered. The τ_d values were calculated as 7.9 μ s and 4.0 μ s for 5 mW and 10 mW laser irradiation, respectively. A criterion was required for the judgment whether two photon signals with a time interval (Δt) were caused by one DiI molecule or not. The Δt values were obtained as 0.70 ms and 0.35 ms for 5 mW and 10 mW laser output, respectively, corresponding to the τ_d values.

When there were many DiI molecules (11 molecules on average) in the observation area, continuous photon signals were observed. Figure 22(a) shows a result of detection for single DiI molecules at the dodecane–water interface; a clear intermittent photon bundle was observed in comparison with the background (Fig. 22(d)). Since DiI molecules are adsorbed at the interface as shown in Fig. 21, the diffusion of DiI is restricted in the lateral direction at the interface, as schematically illustrated in Fig. 22. Therefore, the duration of the photon bundles corresponded to the period in which the single DiI molecule was moving in the observation area. It was assumed that the maximum duration of the photon bundles (t_{\max}) corresponded to the maximum period in which a single DiI molecule stayed in the observation area. In other words, t_{\max} was the period, in which the single molecule moved along the diameter of the round observation area. The lateral diffusion coefficient (D_1) of DiI at the single molecule level was calculated with the equation:

$$D_1 = \frac{d_{\text{obs}}^2}{2t_{\max}} \quad (28)$$

The radius (r) and the diffusion coefficient (D) of a spherical molecule are related to the viscosity (η) of the medium surrounding the molecule with the Einstein-Stokes equation as:

$$D = \frac{kT}{6\pi r\eta} \quad (29)$$

where k is the Boltzmann constant, and T is the absolute temperature. The radius of DiI molecule was estimated as 7.0×10^{-10} m as a sphere from the molecular volume of DiI. The apparent interfacial viscosities ($\bar{\eta}_i$) evaluated with Eq. 29 are listed in Table 6. In the surfactant-free system, the calculated viscosity of 1.4 mPa s was close to the value of dodecane (1.4 mPa s) and it was higher than water (0.89 mPa s). This result suggested that the two long alkyl-groups were immersed deeply in the dodecane phase, as shown in Fig. 20, and governed the $\bar{\eta}_i$ value.

The effect of SDS was examined in the interfacial concentrations of 2.0×10^{-10} and 2.49×10^{-10} mol/cm², which were close to the saturated interfacial concentration of 2.5×10^{-10} mol/cm². The average number of DiI molecules was 0.1 in the observation area. Figures 22(b) and (c) represent examples of the observed photon bundles in the SDS system. The duration of the photon bundle was as wide as that in the surfactant-free system. The D_1 and $\bar{\eta}_i$ values, listed in Table 6, were little affected by the interfacial SDS, regardless of the nearly saturated interfacial concentration of SDS. This means that the translational motion of interfacial SDS molecules is similar to that of dodecane molecules, which is consistent with the fact that both have a dodecyl chain.

Since the phase transition temperature of DMPC is 23 °C,

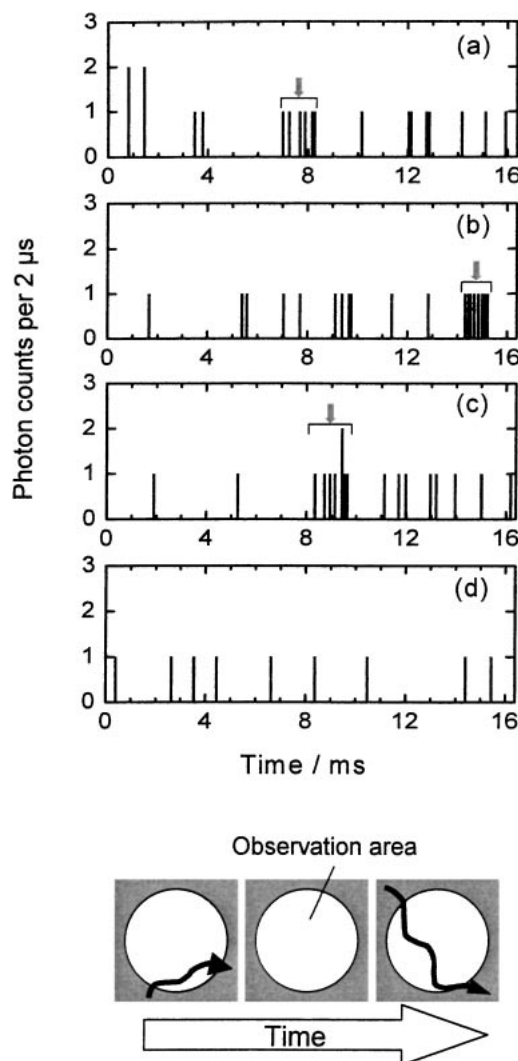


Fig. 22. Observed photon bundles of single DiI molecules (a) at the free dodecane–water interface and (b, c) at the SDS-modified dodecane–water interface for $2 \mu\text{s} \times 8192$ channels measurement. Axes in (a), (b), and (c) indicate photon bundles. The average number of DiI molecules in the observation area were 0.1 for (a), (b), and (c); 0 for (d). Interfacial SDS concentration: (b), 2.0×10^{-10} mol/cm²; (c), 2.49×10^{-10} mol/cm²; (d), 0 mol/cm² (background). 5 mW laser output. Schematic illustration of a trajectory of single DiI molecules at the dodecane–water interface, which is crossing the observation area. Intermittent photon bundles observed in Figs. 22(a)–(c) correspond to the crossing of one DiI molecule in the observation area.

DMPC is in the liquid-like characteristics under the present experimental temperature (25 °C). The average number of DiI molecules in the observation area was less than 0.1. Figure 23(a) displays an example at the highest interfacial concentration of DMPC (2.0×10^{-10} mol/cm²). The threshold level was set to 50 counts for the criterion of the single DiI molecule measurement, since the averaged noise level was about 25 counts as shown in Fig. 23(a). Figures 23(b)–(d) show the expanded figures at three points of Fig. 23(a). In Fig. 23(b), there

Table 6. Effects of Surfactants on the Lateral Diffusion Coefficient (D_l) of Single DiI Molecules, Apparent Viscosity ($\bar{\eta}_i$) and Intrinsic Viscosity (η_i) at the Dodecane–Water Interface, and Fluorescence Quantum Yield (ϕ_f)

Surfactant	Γ_s^a /mol cm ⁻²	D_l /cm ² s ⁻¹	$\bar{\eta}_i$ /mPa s	η_i /mPa s	$\phi_f^{b)}$
Free		2.3×10^{-6}	1.4		0.12
SDS	2.0×10^{-10}	1.7×10^{-6}	1.8	— ^{c)}	0.12
	2.5×10^{-10}	1.6×10^{-6}	1.9	— ^{c)}	0.13
DMPC	2.0×10^{-12}	2.1×10^{-7}	15	37	0.05
	2.0×10^{-11}	4.3×10^{-8}	72	270	0.03
	9.0×10^{-11}	2.7×10^{-8}	120	470	0.02
	2.0×10^{-10}	1.8×10^{-8}	170	750	0.05

a) Interfacial concentration of surfactant. b) $\phi_f = 0.15$ in ethanol. c) Too low to be evaluated.

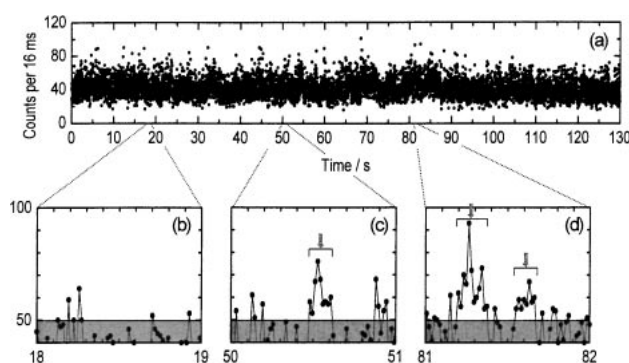


Fig. 23. Examples of photon bundles of single DiI molecules at the dodecane–water interface modified by 2.0×10^{-10} mol/cm² DMPC for 16 ms \times 8192 channels measurement. (a), overall result; (b)–(d), expanded samples. Axes in (c) and (d) indicate photon bundles. Average DiI molecules in the observation area were 0.1. 10 mW laser output power.

were no definite signals beyond the threshold level, indicating that no DiI molecules went across the observation area. In Figs. 23(c) and (d), some photon bundles were observed. The width of the photon bundle increased with the increase in the interfacial DMPC concentration. A histogram of the photon number per one channel obeyed the Poisson distribution that had a large background peak (no DiI) and a small signal peak (one DiI). The D_l and $\bar{\eta}_i$ values of DiI were also listed in Table 1. The maximum $\bar{\eta}_i$ value in the DMPC system was 0.184 Pa s, which was higher than the surfactant-free interface by two orders of magnitude. DMPC is a composition of biological cell membrane and it has a self-organizing nature due to a hydrophobic zwitter ion.

A hydrodynamic model could evaluate the intrinsic viscosity (η_i) of the surfactant monolayer, eliminating the contribution of the viscosity of dodecane and aqueous phases. The η_i values listed in Table 1 were about 2–4 times higher than the apparent $\bar{\eta}_i$. The maximum η_i value was 0.75 Pa s, which was comparable to that of a common viscous liquid, glycerin (0.945 Pa s). The interfacial viscosity increased with the increase in the interfacial concentration of DMPC. This study is the first example that the hydrodynamic properties of the interface has been measured by a single molecule probing.

Conclusion

From the interfacial mechanism in the solvent extraction of metal ions to the single molecule probing of the nano-properties of the interface, recent advances in the nano-chemistry of liquid–liquid interfaces, which have been done mainly in our group, were reviewed. The following points will be summarized as the specific features of the interfacial properties and the interfacial reactions:

- 1) A catalytic role of the interface was recognized in various liquid–liquid extraction systems. Interfacial adsorption of reactants was the key step in the interfacial catalysis. Some guidelines proposed here are useful, not only in the solvent extraction but also in interfacial synthesis.
- 2) Interfacial adsorption of molecules or ions produces a concentrated situation for the species, which is ready to proceed to the formation of aggregates of the species at the interface. Aggregates of metal complex exhibited a unique function as a molecular recognizing reagent. The aggregated state is similar to a cluster state, in which the monomer molecules are closely packed at the two-dimensional interface. In such a state, the selectivity in the structural recognition for isomers was promoted.
- 3) The study on the rotational and translational motion of molecules at the interface supported the fast interfacial reaction rate observed in some solvent extraction systems. Furthermore, the difference in the effect of a single chained surfactant (SDS) and a double chained surfactant (DHP and DMPC) on the reactivity of the adsorbed molecules was indicated. The double chained surfactant will reduce the reactivity or diffusivity of the molecule coexisting at the interface. Single-molecule probing at the interface is a promising means of the measurements of nano-properties of the interface. This approach should be extended to various other systems.
- 4) The usefulness of the microscopic spectrometry and the evanescent spectroscopy was demonstrated. The fluorescence method is now the most versatile and sensitive detection method of the interfacial species, but the Raman spectrometry is also utilized as a more deterministic method. In the development of the measurement method of interfacial reactions, an invention to make a small and thin two phase system is the most important point.

The structure of the liquid–liquid interfaces is still obscure. In the equilibrium, the interface is thought to be flat on the molecular scale.¹⁰ However, in the circumstances including mass transfer, solvent clusters are generated in the nano-region of the liquid–liquid interface.⁹⁹ The liquid–liquid interface has still many fundamental subjects to be studied. Extensive studies from physical, chemical and biological viewpoints are highly required in this research field.

Besides the works cited above, there are many excellent works in relation to the interfacial nano-chemistry in liquid–liquid systems, which have been published in some new books.^{4,36,100}

This study was in part supported financially by the Scientific Research of Priority Areas “Nano-Chemistry at the Liquid–

Liquid interfaces” and a Grant-in-Aid for Scientific Research (A) (No. 12304045) from the Ministry of Education, Culture, Sports, Science and Technology.

References

- 1 I. Benjamin, *J. Phys. Chem.*, **95**, 6675 (1991).
- 2 P. R. Danesi, in “Principles and Practices of Solvent Extraction,” ed by J. Rydberg, C. Musikas, and G. R. Choppin, Marcel Dekker, New York (1992), pp. 157–207.
- 3 H. Watarai, *Trends in Anal. Chem.*, **12**, 3, 13 (1993).
- 4 H. Watarai, in “Liquid Interfaces in Chemical, Biological, and Pharmaceutical Applications,” ed by A. G. Volkov, Marcel Dekker, New York (2000), pp. 355–372.
- 5 H. Watarai and H. Freiser, *J. Am. Chem. Soc.*, **105**, 189 (1983).
- 6 H. Watarai and H. Freiser, *J. Am. Chem. Soc.*, **105**, 191 (1983).
- 7 H. Nagatani and H. Watarai, *Anal. Chem.*, **68**, 1250 (1996).
- 8 H. Watarai and Y. Chida, *Anal. Sci.*, **10**, 105 (1994).
- 9 H. Watarai and Y. Saitoh, *Chem. Lett.*, **1995**, 283.
- 10 S. Ishizaka and N. Kitamura, *Bull. Chem. Soc. Jpn.*, **74**, 1883 (2001).
- 11 H. Nagatani and H. Watarai, *Anal. Chem.*, **70**, 2860 (1998).
- 12 T. Tokimoto, S. Tsukahara, and H. Watarai, *Chem. Lett.*, **2001**, 204.
- 13 G. J. Hanna and R. D. Noble, *Chem. Rev.*, **85**, 583 (1985).
- 14 H. Watarai, M. Gotoh, and N. Gotoh, *Bull. Chem. Soc. Jpn.*, **70**, 957 (1997).
- 15 A. Ohashi and H. Watarai, *Anal. Sci.*, **17**, 1313 (2001).
- 16 H. Nagatani and H. Watarai, *Chem. Lett.*, **1999**, 701.
- 17 A. Ohashi and H. Watarai, *Chem. Lett.*, **2001**, 1238.
- 18 H. Nagatani and H. Watarai, *Anal. Chem.*, **68**, 1250 (1996).
- 19 G. D. Owens, R. W. Taylor, T. Y. Ridley, and D. W. Margerum, *Anal. Chem.*, **52**, 130 (1980).
- 20 H. Watarai and F. Funaki, *Langmuir*, **12**, 6717 (1996).
- 21 S. Tsukahara, Y. Yamada, T. Hinoue, and H. Watarai, *Bunseki Kagaku*, **47**, 945 (1998).
- 22 M. J. Wirth and J. D. Burbage, *J. Phys. Chem.*, **96**, 9022 (1992).
- 23 S. Tsukahara, Y. Yamada, and H. Watarai, *Langmuir*, **16**, 6787 (2000).
- 24 S. Tsukahara and H. Watarai, *Chem. Lett.*, **1999**, 89.
- 25 Y. Moriya, N. Ogawa, T. Kumabe, and H. Watarai, *Chem. Lett.*, **1998**, 221.
- 26 K. Fujiwara and H. Watarai, *Bull. Chem. Soc. Jpn.*, **74**, 1885 (2001).
- 27 H. Nagatani, R. A. Iglesias, D. J. Fermin, P. F. Brevet, and H. H. Girault, *J. Phys. Chem. B*, **104**, 6869 (2000).
- 28 N. Nishi, K. Izawa, M. Yamamoto, and T. Kakiuchi, *J. Phys. Chem. B*, **105**, 8162 (2001).
- 29 H. Nagatani, D. J. Fermin, and H. H. Girault, *J. Phys. Chem. B*, **105**, 9463 (2001).
- 30 K. Nakatani, H. Nagatani, D. J. Fermin, and H. H. Girault, *J. Electroanal. Chem.*, **518**, 1 (2002).
- 31 D. J. Fermin, Z. Ding, P. F. Brevet, and H. H. Girault, *J. Electroanal. Chem.*, **447**, 125 (1998).
- 32 T. Osakai, H. Jensen, H. Nagatani, D. J. Fermin, and H. H. Girault, *J. Electroanal. Chem.*, **510**, 43 (2001).
- 33 T. Kakiuchi and Y. Takasu, *Anal. Chem.*, **66**, 1853 (1994).
- 34 R. M. Corn and D. A. Higgins, *Chem. Rev.*, **94**, 107 (1994).
- 35 K. B. Eisenthal, *Chem. Rev.*, **96**, 1343 (1996).
- 36 P.-F. Brevet and H. H. Girault, in “Liquid–Liquid Interfaces, Theory and Methods,” ed by A. G. Volkov and D. W. Deamer, CRC Press, Boca Raton, FL (1996), Chap. 6, p. 103.
- 37 D. A. Higgins and R. M. Corn, *J. Phys. Chem.*, **97**, 489 (1993).
- 38 H. F. Wang, E. Borguet, and K. B. Eisenthal, *J. Phys. Chem. A*, **101**, 713 (1997).
- 39 H. F. Wang, E. Borguet, and K. B. Eisenthal, *J. Phys. Chem. B*, **102**, 4927 (1998).
- 40 R. R. Naujok, D. A. Higgins, D. G. Hanken, and R. M. Corn, *J. Chem. Soc., Faraday Trans.*, **91**, 1411 (1995).
- 41 R. R. Naujok, H. J. Paul, and R. M. Corn, *J. Phys. Chem.*, **100**, 10497 (1996).
- 42 A. A. T. Luca, P. Hebert, P.-F. Brevet, and H. H. Girault, *J. Chem. Soc., Faraday Trans.*, **91**, 1763 (1995).
- 43 N. Teramae, T. Uchida, A. Yamaguchi, K. Nochi, T. Yamashita, and T. Shioya, *Bunseki Kagaku*, **48**, 1063 (1999).
- 44 J. Rinuy, A. Piron, P. F. Brevet, M. B-Desce, and H. H. Girault, *Chem.-Eur. J.*, **6**, 3434 (2000).
- 45 A. Piron, P. F. Brevet, and H. H. Girault, *J. Electroanal. Chem.*, **483**, 29 (2000).
- 46 R. W. Boyd, “Nonlinear Optics,” Academic Press, London (1992).
- 47 R. L. Sutherland, “Handbook of Nonlinear Optics,” Marcel Dekker, New York (1996).
- 48 P.-F. Brevet, “Surface Second Harmonic Generation,” Presses Polytechniques et Universitaires Romandes, Lausanne (1997).
- 49 H. Watarai, A. Matsumoto, and T. Fukumoto, *Anal. Sci.*, **18**, 367 (2002).
- 50 F. Hashimoto, S. Tsukahara, and H. Watarai, *Anal. Sci.*, **17**, i81 (2001).
- 51 H. Watarai and K. Satoh, *Langmuir*, **10**, 3913 (1994).
- 52 H. Watarai, M. Takahashi, and K. Shibata, *Bull. Chem. Soc. Jpn.*, **59**, 3469 (1986).
- 53 H. Watarai and M. Endo, *Anal. Sci.*, **7**, 137 (1991).
- 54 Y. Onoe and H. Watarai, *Anal. Sci.*, **14**, 237 (1998).
- 55 H. Watarai and Y. Onoe, *Solvent. Extr. Ion Exch.*, **19**, 155 (2001).
- 56 Y. Yulizar, A. Ohashi, and H. Watarai, *Anal. Chim. Acta*, **447**, 247 (2001).
- 57 A. Ohashi and H. Watarai, *Chem. Lett.*, **32**, 218 (2003).
- 58 A. Ohashi, S. Tsukahara, and H. Watarai, *Anal. Chim. Acta*, **364**, 53 (1998).
- 59 T. Tokimoto, S. Tsukahara, and H. Watarai, *Anal. Sci.*, **17**, i1245 (2001).
- 60 H. Watarai, *J. Phys. Chem.*, **89**, 384 (1985).
- 61 H. Watarai, *Talanta*, **32**, 817 (1985).
- 62 H. Watarai and Y. Shibuya, *Bull. Chem. Soc. Jpn.*, **62**, 3446 (1989).
- 63 H. Watarai, K. Sasaki, and N. Sasaki, *Bull. Chem. Soc. Jpn.*, **63**, 2797 (1990).
- 64 Y. Chida and H. Watarai, *Bull. Chem. Soc. Jpn.*, **69**, 341 (1996).
- 65 Y. Saitoh and H. Watarai, *Bull. Chem. Soc. Jpn.*, **70**, 351 (1997).
- 66 R. Okumura, T. Hinoue, and H. Watarai, *Anal. Sci.*, **12**, 393 (1996).
- 67 K. Fujiwara and H. Watarai, *Langmuir*, **19**, 2658 (2003).
- 68 B. Freiser and H. Freiser, *Talanta*, **17**, 540 (1970).
- 69 H. Watarai, K. Sasaki, K. Takahashi, and J. Murakami, *Talanta*, **42**, 1691 (1995).

- 70 H. Watarai, K. Takahashi, and J. Murakami, *Solv. Extr. Research Develop. Jpn.*, **3**, 109 (1996).
- 71 Y. Onoe, S. Tsukahara, and H. Watarai, *Bull. Chem. Soc. Jpn.*, **71**, 603 (1998).
- 72 M. Fujiwara, S. Tsukahara, and H. Watarai, *Phys. Chem. Chem. Phys.*, **1**, 2949 (1999).
- 73 N. Fujiwara, S. Tsukahara, and H. Watarai, *Langmuir*, **17**, 5337 (2001).
- 74 N. Fujiwara, S. Tsukahara, and H. Watarai, *Anal. Sci.*, **17**, i231 (2001).
- 75 A. Ohashi, S. Tsukahara, and H. Watarai, *Anal. Chim. Acta*, **394**, 23 (1999).
- 76 A. Ohashi and H. Watarai, *Langmuir*, **18**, 10292 (2002).
- 77 A. Ohashi, S. Tsukahara, and H. Watarai, *Langmuir*, **19**, 4645 (2003).
- 78 T. Kakiuchi, in "Liquid-Liquid Interfaces, Theory and Methods," ed by A. G. Volkov and D. W. Deamer, CRC Press, Boca Raton, FL (1996), p. 1, Chap. 1.
- 79 K. Maeda and S. Kihara, *Bull. Chem. Soc. Jpn.*, **70**, 1505 (1997).
- 80 H. Nagatani, Z. Samec, P.-F. Brevet, D. J. Fermin, and H. H. Girault, *J. Phys. Chem. B*, **107**, 786 (2003).
- 81 H. Nagatani, A. Piron, P. F. Brevat, D. J. Fermin, and H. H. Girault, *Langmuir*, **18**, 6647 (2002).
- 82 K. S. Suslick, C. T. Chen, G. R. Meredith, and L. T. Cheng, *J. Am. Chem. Soc.*, **114**, 6928 (1992).
- 83 A. Sen, P. C. Ray, P. K. Das, and V. Krishnan, *J. Phys. Chem.*, **100**, 19611 (1996).
- 84 D. A. Piasecki and M. J. Wirth, *J. Phys. Chem.*, **97**, 7700 (1993).
- 85 S.-H. Chou and M. J. Wirth, *J. Phys. Chem.*, **93**, 7694 (1989).
- 86 L. A. M. Rupert, J. F. L. van Breemen, D. Hoekstra, and J. B. F. N. Eugberts, *J. Phys. Chem.*, **92**, 4416 (1988).
- 87 P. Walde, M. Wessicken, U. Rädler, N. Berclaz, K. Conde-Frieboes, and P. L. Luisi, *J. Phys. Chem. B*, **101**, 7390 (1997).
- 88 J. T. Petkov, K. D. Danov, and N. D. Dankov, *Langmuir*, **12**, 2650 (1996), and references therein.
- 89 P. R. Briley, A. R. Deemer, and J. C. Slattery, *J. Colloid Interface Sci.*, **56**, 1 (1976).
- 90 S. Tsukahara and H. Watarai, *Langmuir*, **14**, 7072 (1998).
- 91 S. Nie, D. T. Chiu, and R. N. Zare, *Anal. Chem.*, **67**, 2849 (1995).
- 92 T. Funatsu, Y. Harada, M. Tokunaga, K. Saito, and T. Yanagida, *Nature*, **374**, 555 (1995).
- 93 M. Tokunaga, K. Kitamura, K. Saito, A. H. Iwane, and T. Yanagida, *Biochem. Biophys. Res. Commun.*, **235**, 47 (1997).
- 94 D. C. Nguyen, R. A. Keller, J. H. Jett, and J. C. Martin, *Anal. Chem.*, **59**, 2158 (1987).
- 95 M. Ishikawa, K. Hirano, T. Hayakawa, S. Hosoi, and S. Brenner, *Jpn. J. Appl. Phys.*, **33**, 1571 (1994).
- 96 M. J. Wirth and D. J. Swinton, *Anal. Chem.*, **70**, 5264 (1998).
- 97 S. Ho Kang, M. R. Shortreed, and E. S. Yeung, *Anal. Chem.*, **73**, 1091 (2001).
- 98 F. Hashimoto, S. Tsukahara, and H. Watarai, *Langmuir*, **19**, 4197 (2003).
- 99 A. Pfennig, *Chem. Eng. Sci.*, **55**, 5333 (2000).
- 100 "Interfacial Catalysis," ed by A. G. Volkov, Marcel Dekker, NY (2003).
- 101 K. Akiba and H. Freiser, *Anal. Chim. Acta*, **136**, 339 (1982).



Hitoshi Watarai, Professor of Analytical Chemistry, Department of Chemistry, Graduate School of Science, Osaka University, was born in 1947 in Yamagata Pref. He was trained in the field of Physical Chemistry (Photochemistry) and received a B.Sc. (1969) and a M.Sc. (1971) from Tohoku University. He was employed as a Research Associate (1971) in Tohoku University, Analytical Chemistry Laboratory, Department of Chemistry, and received a D.Sc. (1978) from Tohoku University. From 1981 to 1982, he worked as a Research Associate in the laboratory of Professor Henry Freiser, Department of Chemistry, The University of Arizona, studying the role of interfaces in solvent extraction kinetics. He was appointed as Lecturer (1982), an Associate Professor (1983), and a Professor (1988) in the Faculty of Education of Akita University. In 1993, he moved to Osaka University, Faculty of Science (from 1996, the Graduate School of Science). His research interest covers "Nano-chemistry at the liquid-liquid interface" and "Creation of new migration analysis of microparticles." He received The Divisional Award of The Chemistry Society of Japan for 2000.



Satoshi Tsukahara was born in Ibaraki, Japan, in 1964. After graduating from Tohoku University in 1986, he entered the Graduate School of this University. He got his M.S. degree from Tohoku University in 1988. He withdrew from the Graduate School in August in 1988, and he became a Research Assistant at Tohoku University in September in 1988. In 1993, he received his degree of D.Sc. through the submission of his dissertation at Tohoku University under the direction of Professor Nobuo Suzuki. In 1995, he moved to Graduate School of Science, Osaka University as a Research Assistant and became a Lecturer in 2003. His research interests are chemical reaction dynamics at liquid-liquid interface and dielectrophoresis of microparticles in non-uniform electric fields. He received The Japan Society for Analytical Chemistry award for younger researchers in 1998.



Hirohisa Nagatani, Research Associate of the Department of Natural Sciences, Hyogo University of Teacher Education, Japan was born in 1971. He received his B.Eng. in 1994 from Ryukoku University and M.Sc. in 1996 and D.Sc. in 1999 from Osaka University. He has been a JSPS Research Fellow in Osaka University since 1998. In 1999, he joined Professor Hubert H. Girault's group of Ecole Polytechnique Fédérale de Lausanne (EPFL), Switzerland as a JSPS Research Fellow and as an Assistant since 2001. Then he moved to his current position at 2002. His research activities include spectro-electrochemical study of adsorption reaction of functional dyes at the liquid-liquid interface.



Akira Ohashi was born in Aichi in 1973. He graduated from the Department of Chemistry, Faculty of Science, Osaka University, in 1997, and received his M.S. degree (1999) and D.S. degree (2002) from the same university. He was given a Research Fellowship for Young Scientists from the Japan Society for the Promotion of Science (1999–2001). He was promoted to a Research Associate at Ibaraki University in 2002. His research interests include the aggregations of metal chelate at the liquid-liquid interface and chemical reactions at the supercritical carbon dioxide-water interface.